Student thesis series INES nr 582

Evaluating forest wildfire effect on tree increment patterns for boreonemoral forests in Sweden

- A pilot study using remote sensing

Joanna Eaton

2022
Department of
Physical Geography and Ecosystem Science
Lund University
Sölvegatan 12
S-223 62 Lund
Sweden

Joanna Eaton (2022).
Evaluating forest wildfire effect on tree increment patterns for the boreonemoral forest in Sweden. – A pilot study using remote sensing.
Bedömning av skogsbrandseffekt på träd tillväxt mönster för boreonemoerala skogar i Sverige. – En pilotstudie med användning av fjärranalys.
Master degree thesis, 30 credits in *Atmospheric science and biogeochemical cycles*
Department of Physical Geography and Ecosystem Science, Lund University

Level: Master of Science (MSc)

Course duration: *January* 2022 until *June* 2022

Evaluating forest wildfire effect on tree increment patterns for boreonemoral forests in Sweden

- A pilot study using remote sensing

Joanna Eaton

Master thesis, 30 credits, in *Atmospheric science and biogeochemical cycles MSc**

Veiko Lehsten
Dep. of Physical Geography and Ecosystem Science, Lund University

Johan Eckdahl
Ph.D. Student in the Dep. of Physical Geography and Ecosystem Science, Lund University

Exam committee:
Martin Berggren
Dep. of Physical Geography and Ecosystem Science, Lund University

John Bergkvist
Dep. of Physical Geography and Ecosystem Science, Lund University

Abstract

The release of anthropogenic greenhouse gases (GHGs) has substantially increased the global mean surface air temperature. Increases in global mean surface air temperature will lead to warmer and drier conditions, promoting more frequent, long-lasting, intense forest wildfires. The usage of remote sensing (RS) can aid in quantifying forest characteristics and large-scale changes in forest ecosystems. RS can detect wildfires, assess the damage level of burnt forests, and enhance the evaluation of forest regeneration after a fire event. Differenced normalized burn ratio (dNBR), Normalized differential vegetation index (NDVI), and differenced normalized difference vegetation index (dNDVI) have been proven to assess forest fire disturbance and forest health. However, many of these techniques have yet to be validated by field sampling in Swedish boreonemoral forest systems.

The study aimed to investigate and evaluate the existing RS methodology for fire disturbance and forest health in a group of Swedish boreonemoral forests. This was done by using the proposed RS methodology and dendrochronology assessment. Estimating burn severity (dNBR) and forest health (dNDVI) on boreonemoral forests show good potential as the fire disturbance signal and health of the forest are captured using Sentinel-2 images. This study concluded that using the presented RS methodology for visualisation (dNBR and dNDVI) is viable as it helps users visualise the effects and severity of boreal forest wildfires and vegetation recovery. Using dNBR as a tool to estimate burn severity patterns has been proven possible but unreliable regarding the relationship between high burn severity and decreased tree increment patterns. NDVI temporal changes have been shown to explain some of the changes to Pine increment patterns but are restricted to 1–2-year trends. However, NDVI might be reliable for evaluating temporal growth increment patterns in Swedish boreonemoral forests. Due to the few sites, this cannot be confirmed or denied. Both presented RS methods are robust but need modifying as variabilities in reflectance can be an uncertainty. The usage of the used RS methodology shows potential for further studies, as improvements can be made from this study to validate the presented method and assessment better.

Keywords: Remote sensing, dNBR, NDVI, dNDVI, Dendrochronology

Sammanfattning

Utsläppet av de antropogena växthusgaser (GHG) har avsevärt ökat den globala medeltemperaturen. Ökning av den globala medeltemperaturen kommer leda till varmare och torrare förhållanden, vilket främjar mer frekventa långvariga intensiva skogsbränder. Användningen av fjärranalys (RS) kan hjälpa till att kvantifiera skogens egenskaper och storskaliga förändringar i skogens ekosystem. RS kan upptäcka skogsbränder, bedöma skadenivån på brända skogar och förbättra utvärderingen av skogsåterhämtning efter en brandhändelse. Tidigare forskning har påvisat att differentierat normaliserat bränn förhållande (dNBR), normaliserat differentiellt vegetationsindex (NDVI) och differentierat normaliserat differensvegetationsindex (dNDVI) kan användas för att bedöma störningar orsakat av skogsbränder och skogsåterhämtning. Många av dessa tekniker har dock ännu inte validerats genom fältprovtagning i svenska boreonemoerala skogssystem.

Studien syftade till att undersöka och utvärdera den befintliga RS-metodiken för brandstörning och skogsåterhämntning i en grupp svenska boreonemoerala skogar. Detta gjordes genom att använda den föreslagna RS-metoden och dendrokronologiska metodiken. Uppskattning av brännskador (dNBR) och skogshälsa (dNDVI) på boreonemoerala skogar visar god potential eftersom brandstörningssignalen och skogsåterhämtning fångas med Sentinel-2-bilder. Denna studie drog slutsatsen att det är lönsamt att använda den presenterade RS-metoden för visualisering (dNBR och dNDVI), eftersom den hjälper användare att visualisera effekterna och brand störningsgraden av boreala skogsbränder och återhämtning av vegetation. Att använda dNBR som ett verktyg för att uppskatta mönster för brännskador har visat sig vara möjligt men inte tillförlitligt när det gäller sambandet mellan hög brännskada och minskade mönster för trädtillväxt. NDVI-tidsförändringar har visat sig förklara några av förändringarna i tall tillväxtsmönster men är begränsade till 1–2-åriga trender. Däremot kan NDVI vara en tillförlitlig metod för att utvärdera temporala tillväxttillväxtmönster i svenska boreonemoerala skogar. På grund av de få studieplatserna kan detta inte bekräftas eller förnekas. De presenterade RS-metoderna är robusta men behöver modifieras eftersom variationer i reflektans kan vara en osäkerhet. Användningen av den presenterade RS-metoden visar potential för ytterligare studier, eftersom förbättringar kan göras från denna studie för att bättre validera den presenterade metodiken och bedömningen.

Nyckelord: Fjärranalys, dNBR, NDVI, dNDVI, Dendrokronologi

Acknowledgements

I owe my most incredible gratitude to my supervisor Veiko Lehsten, for his knowledge, guidance, encouragement, and support throughout the thesis course. I also want to thank my co-supervisor, Johan Eckdahl, for his patience, advice, and guidance.

Additionally, I would like to extend my gratitude to Johannes Edvardsson, who guided me with his experience and knowledge in dendrochronology. Lastly, I want to thank Wenxin Zhang for his expertise and help in RS processing in MATLAB.

Also, a special thanks to the BECC's project; without this the thesis would not be possible.

Thank you.

BECC is a collaboration project between Lund University and Gothenburg University. BECCs aim to tackle the challenges of social-ecological complexes with connections to climate change and land-use change and how these affect biodiversity and ecosystem services. BECC also focuses on direct and indirect human impacts on the climate and its ecosystem and how these affect biodiversity and ecosystem functioning on a local to global scale.

Table of Contents:

1. Introduction

The release of anthropogenic greenhouse gases (GHGs) has substantially increased the global mean surface air temperature, with further increases predicted should mitigation measures fail to be enacted (IPCC, 2019; IPCC, 2021). This is of great concern as the planet's warming can trigger various positive feedback mechanisms that can further amplify climate change (IPCC, 2019; IPCC, 2021). One feedback of increasing concern is climate-amplified forest wildfire activity.

Forest wildfires are naturally occurring fires in forest ecosystems that are non-prescribed. These fires can potentially release large amounts of GHGs through the combustion of vegetation and soil and can be extremely difficult to control (Martell, 2007; UN, 2022; Global Forest Watch, 2022). Increases in global mean surface air temperature, along with the frequency and extremity of drought conditions, enhance the flammability of forest ecosystems (Martell, 2007; Alkhatib, 2014; Holden, et al., 2016; Sherstjuk, et al., 2018; IPCC, 2021; UN, 2022). Warmer and drier conditions and poor land management promote frequent, long-lasting, and more intense wildfires (Sunar & Özkan, 2001; Martell, 2007; Global Forest Watch, 2022). Of the GHGs emitted during wildfire events, carbon (C) containing compounds have the most substantial impact on the climate due to their relative abundance and long atmospheric lifetimes (Akther & Hassan, 2011; Alkhatib, 2014; Holden, et al., 2016). Previous studies have shown that boreal forest fires can enhance forest biodiversity depending on the burn severity. However, they can also harm boreal forest ecosystems as they act as a net C sink.

The usage of remote sensing (RS) can aid in quantifying forest characteristics and large-scale changes in forest ecosystems (White, et al., 1996; Isaev, et al., 2002; Sherstjuk, et al., 2018). RS can help detect wildfires, assess the damage level of burnt forests, calculate global burned areas, and enhance the evaluation of forest regeneration after a fire event (White, et al., 1996; Isaev, et al., 2002; Chuvieco, et al., 2004; Akther & Hassan, 2011; Eriksson, et al., 2018; Sherstjuk, et al., 2018). Several studies have assessed the correlation between normalised difference vegetation index (NDVI) and tree ring width growth (Kaufmann, et al., 2008; Bhuyan, et al., 2017). The results revealed a positive correlation between the tree rings' width and high NDVI values for the summer months in boreal forests (Kaufmann, et al., 2008; Bhuyan, et al., 2017). Damaged or dead vegetation will show more reflectance in the red region of the visible spectrum and thus will have a lower NDVI. Thus, applying NDVI to RS for vegetation health estimation, pre-fire and post-fire, should be able to explain the loss of "greenness" from forests after a wildfire event.

Burn severity application to RS is another way of assessing wildfires, as they can provide detailed information regarding the fire perimeters, intensity, and severity (Whitman, et al., 2018; UN, 2022). Differenced normalised burn ratio (dNBR), like NDVI, uses spectral bands to assess changes in reflectance from wildfire-affected

areas. The shift in dNBR from pre- to post-fire can help evaluate the severity of the fire during and after the event: high severity will show a higher value (+1) while low severity (often correlated with regrowth) will show lower to negative values and thus give an insight to the intensity of the fire (Whitman, et al., 2018; UN, 2022).

An increase in wildfire regimes will release more significant portions of stored C in soil and biomass as fires are one of the more dominating factors of the in-time rapid release of C back into the atmosphere. Thus, it is essential to utilise satellite imagery to better understand and improve the global C budget from boreonemoral ecosystems. dNBR, dNDVI, and NDVI have been proven to address this issue, but with lacking validation from ground measurements, it is still uncertain how well they perform in Swedish boreonemoral biomes. Thus, RS can be a powerful tool for boreal and boreonemoral wildfire evaluation and assessment in these ecosystems around the globe.

2. Aim

This study aims to investigate and evaluate the existing RS methodology for fire disturbance and forest health in a group of Swedish boreonemoral forests. Sweden's altered fire regime and its relative lack of wildfire sampling deserve separate validation of related satellite imagery.

This project is part of the Lund University collaboration with BECCs under the physical geography and ecosystem science department. This study is a pilot study for the project *Learning from a fire-prone past for a fire-prone future: Assessing the effect of forest fires (pilot project)* in BECCs.

This study intends to address the following hypotheses regarding the application of RS to boreal forest wildfires in Sweden:

1. *dNBR can be used to assess the 2018 boreonemoral forest wildfire activity.*
2. *A correlation between high burn severity and low tree increment pattern can be established.*
3. *dNDVI can be used to assess the health of boreonemoral forests after the 2018 wildfire activity.*
4. *NDVI can explain temporal changes to tree increment patterns for Pinus sylvestris.*

3. Theoretical Background

3.1. Fennoscandian Climate and Biome

The Fennoscandian region varies climatically and ecologically (Karlsen, et al., 2009). The Scandinavian peninsula in Fennoscandia owns much of its weather due to the maritime climate, where warm moisture-rich prevailing westerlies and southwesterlies originate from the North Atlantic (Skartveit, et al., 1975). Scandinavia is also affected

by the arctic south-directed cold airmasses that produce long-lasting clouds, creating a climatically diverse region (Skartveit, et al., 1975). The amount of precipitation that falls in the area is heavily determined by the quantity of moisture released from the westerlies and southwesterlies (Skartveit, et al., 1975).

Moen and Lillethun (1999) divided the Fennoscandian biome into vegetation zones representing the dominating species (Figure 1). The boreonemoral zone is the transition zone between deciduous broad-leaved forest and coniferous forests, which dominates Sweden's middle to the southern area (Moen & Lillethun, 1999; Karlsen, et al., 2009). The transition zone from boreonemoral to the northern boreal zones is coniferous-dominated (Økland, 1990; Esseen, et al., 1992; Moen & Lillethun, 1999; Karlsen, et al., 2009). The start of the growing season for the Fennoscandian climate varies, where the southern nemoral zone can experience lush green forests as early as May-June whilst the northern alpine regions still face snowmelt (Beck, et al., 2007; Høgda, et al., 2013). The start of the growing season is heavily influenced by both abiotic and biotic influences, where the most prominent trigger being the temperature (Beck, et al., 2007).

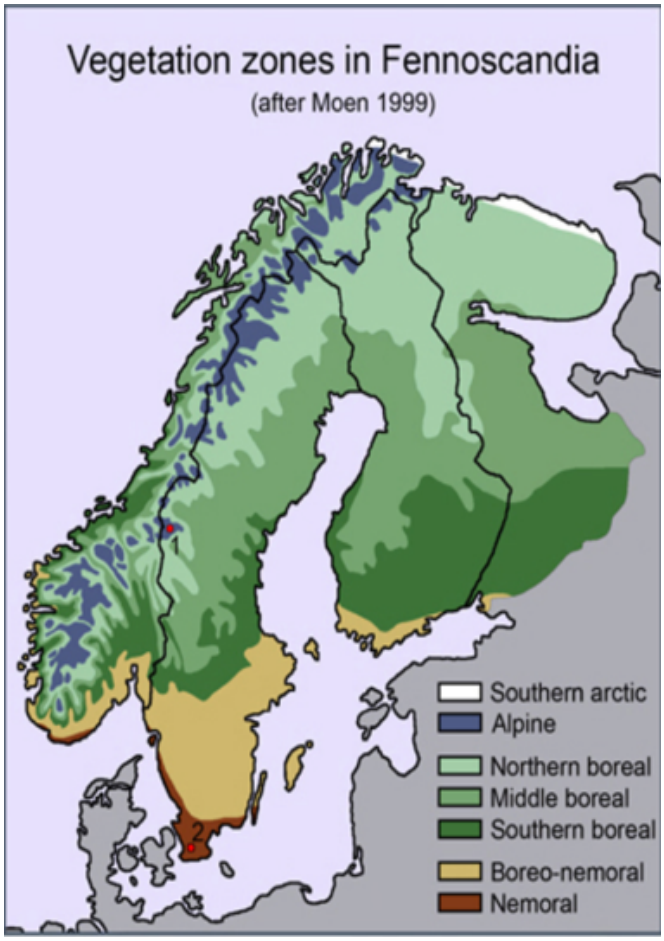

Figure 1: Moen's vegetation zone classification for Fennoscandia (1999).

The Fennoscandian boreal forest structure is considered homogeneous, where *Pinus sylvestris* (Pine) and *Picea abies* (Spruce) is the most dominating species found, where forests cover 65% of the total land area in Sweden alone (Esseen, et al., 1997; Milz,

2013). The two species have a broad habitat amplitude, ranging from dry rocky and alluvial heaths to forest wetlands and mires. Pine trees tend to prevail on drier soils with continental climates with higher fire frequency (Esseen, et al., 1997).

3.2. Forest Fires

"Wildfires are a result of temperature conditions, of soil moisture conditions; and, of course, something has to start it."

By John Holdren 2008

3.2.1. Wildfires

Wildfires are prone to happen during dry seasons, where temperatures are high and soil moisture is low (Bickerton, 2012; Wolters, 2022; WHO, 2022). Such seasons dry out the lush green vegetation converting it to dry combustible fuel. The ignition source for fires can come from human-induced activity (faulty power lines, arson, campfire, to name a few) or natural occurrences like lightning strikes (Bickerton, 2012; Wolters, 2022; WHO, 2022). There is still uncertainty about how wildfires start, around 50% of recorded wildfires, the ignition source is unknown (WHO, 2022). For wildfires to occur, three conditions must be fulfilled: fuel, oxygen, and energy. These three conditions together are known as the fire triangle (Bickerton, 2012; Wolters, 2022; WHO, 2022).

The increase in wildfire intensity and spreading worldwide have caused various damage in different sectors (Chiu, et al., 2022). Around 6.2 million people worldwide get affected by wildfire and volcanic activity each year, where 2400 deaths each year result from direct or secondary impacts. Direct impacts come from burns, suffocations, and injuries, whereas secondary damages can come from inhaling particles. Wildfires impact the climate and ecosystems due to the massive release of carbon dioxide (CO_2), carbon monoxide (CO), and fine particle mattes that get scattered into the atmosphere and transported long distances, altering air quality. Other impacts include infrastructure disruption, food security, loss of crops and animals, and resource loss, to name a few (Shi, et al., 2021; UCDavis, 2022). The ongoing climate change and rapid release of GHGs alter terrestrial ecosystems to favour wildfires. This causes hotter and more intense wildfires worldwide and varies the turnover time for wildfires.

3.2.2. Boreal forest fires

Fire disturbances in boreal ecosystems have been shown to affect the succession dynamics in boreal forests, the carbon dynamics, the age of the forest, and their structure of them (Wallenius, et al., 2004; Kasischke, et al., 2011; Rolstad, et al., 2017; Kuosmanen, et al., 2018). Forest fires at a local scale allow nutrients to be released back into the ecosystem and decrease competitors in the area. This allows favourable conditions for forest regeneration and below-canopy species to establish and change the biodiversity. Forest fires also spatially enhance the site's heterogeneity, allowing

mosaic patterns to form between burned and unburned patches (Wallenius, et al., 2004; Rolstad, et al., 2017). Precursors to boreal forest fires play an essential role in the burning patterns, where vegetation, topography, and slope face, to name a few, can determine why some boreal forest burn compared to others in the same region (Angelstam, 1998).

Fennoscandian boreal forest, dominated by pine, tends to have a fire turnover time of 20-60 years compared to the turnover time for general boreal forests, which tends to be a few decades to around 100-year intervals (Esseen, et al., 1997; Wallenius, et al., 2004; Rolstad, et al., 2017). Pine-dominated forest shows that the fire frequency may be explained by vegetation characteristics and soil moisture found at the site (Wallenius, et al., 2004). However, Fennoscandian fire frequencies might not be correlated with the increase in temperature alone, but rather with soil moisture and other factors (Rolstad, et al., 2017). There is still uncertainty about how Fennoscandian forests' vegetation dynamics get affected by forest wildfires (Molinari, et al., 2020). The uncertainty may lay in the low frequency of Fennoscandian forest fires, as around 0.004% of them annually burns.

3.2.3. 2018 Swedish forest fires

During the summer of 2018, Sweden faced one of the worst fire episodes in the modern day (Björklund, 2019; Granström, 2020). The fire peak of summer 2018 ranged from the 12th to the 20th of July, when the fire weather index (FWI) peaked at over 22 (Granström, 2020). The total amount of forest fires that burned during 2018 is still unclear, only 31 fires were bigger than 50 ha, and seven of them were bigger than 500 ha (Granström, 2020). The most extensive fires during the period were located around southern Norrland and northern Dalarna. The total burn area due to these fires reached 25 000 ha (Björklund, 2019).

The 2018 fires resulted from multiple abiotic factors, one being temperature and the other being precipitation (Rolstad, et al., 2017; Krisinformationen, 2018; Björklund, 2019; Björheden & Johannesson, 2019). During the summer of 2018, the temperatures recorded were one of the highest Sweden has faced in modern days. Most areas of Sweden had an average of < 35ºC (< 95 º F) temperature peaks (hot spells) (Granström, 2020). The number of days with precipitation and rainfall was below average to almost none. This created long periods of extremely high fire risk in Sweden. The reasons for a loss of precipitation and extreme hot spells were the weakened Atlantic jet stream and the high-pressure blocking front (Granström, 2020). This ultimately caused the forests to dry out, revealing combustible fuel from dead wood, grass, and shrubs (Björklund, 2019).

3.3. Sentinel-2 Copernicus mission

Space-borne imagery is a powerful tool to examine Earth's surface and its changes using spectral instruments that measure spectral bands in visible, infrared, and radar frequencies (Segah, et al., 2010). Space-borne imagery has assisted scientists in

estimating and detecting wildfires around the globe. The start and end of wildfires, fire intensity, and the total number of burned areas are still largely unknown. Thus using satellites can help assess this issue (Li, et al., 2010). As boreal fires are one of the more dominating factors of in-time rapid C release from boreal forest ecosystems, it is crucial to utilise satellite imagery to help improve the global C budget (Li, et al., 2010; Kasischke, et al., 2011). One of the first usages of space-borne fire detection comes from using AVHRR data (Kelhä, et al., 2003). Today different satellites can help detect wildfires with the help of the instruments they carry onboard (Milz, 2013). Different satellites deliver different products that can vary spatially and temporally. Among the available satellites, Sentinel-2 Copernicus twin satellites have been used to detect small and largescale wildfires in boreal ecosystems.

Sentinel-2 Copernicus's mission aims to monitor variability in land surface conditions. It comprises twin polar-orbiting satellites with the same sun-synchronous orbits, with a temporal resolution of 2-5 days in mid-latitudes (ESA, u.d.). The twin satellites carry a multispectral instrument providing 13 spectral bands at 10m, 20m, and 60m spatial resolution (ESA, u.d.). Several of the 13 bands provided by Sentinel-2 are burn sensitive, where they lay in the electromagnetic spectrum's visible and shortwave spectral range. One band that has proven to be very useful in estimating the extent of fire damage is the red-edge band. The Sentinel-2 Copernicus mission for fire detection has been used for European countries since its start in 2015 but has also been applied to post-fire monitoring and forest health/regrowth (Farasin, et al., 2020; De Simone, et al., 2020).

3.4. Fennoscandian forest fire estimations

Previous studies have used different indexes to estimate forest health, burn severity, fire damage, forest health, and forest regrowth with the help of RS technology. These indexes are based on calculations using the spectral bands provided by space-borne imagery. Correlations between the indexes and field measurements are accurate depending on the topography, vegetation, and soil moisture (Llorens, et al., 2021).

3.4.1. NBR and dNBR

To estimate burn damage, the index NBR is commonly used (UN, 2022). NBR is calculated by using bands in the near-infrared (NIR) and short-wave infrared (SWIR) regions in the electromagnetic field (Farasin, et al., 2020). NBR considers the NIR and SWIR region as they are less sensitive to atmospheric influences, and thus can more accurately estimate the effects of fire on vegetation (Llorens, et al., 2021; UN, 2022). This index can help map out the burn area and its severity, thus highlighting them. Areas affected by fires have relatively low reflectance in the NIR region and high in the SWIR region (De Simone, et al., 2020). High NBR values (<+1) indicate healthy vegetation. In contrast, low values indicate bare ground or burnt areas, which can pose a problem if a forest has been clearcut as this will display a fire-affected area when using RS.

dNBR, similar to NBR, is an extension of NBR where the NBR values from pre- and post-fire are used to estimate the severity of burn areas from satellite images (Keeley, 2009; Farasin, et al., 2020). Unlike NBR, high values of dNBR (< +1) indicate more damage and inform users of the severity of the fire, while negative numbers (-1<) indicate enhanced forest regrowth (Quintano, et al., 2018).

3.4.2. NDVI and dNDVI

The vegetation index NDVI quantifies vegetation "greenness" by using satellite imagery's red and NIR bands (Lacouture, et al., 2020; GISGeography, 2022). This index allows users to measure vegetation productivity and recovery from natural or human-induced disturbances to forest ecosystems (Segah, et al., 2010; Lacouture, et al., 2020). Vegetation (chlorophyll) absorbs light in the red region of the electromagnetic spectrum. At the same time, it reflects light in the NIR region, thus, reviewing the relationship between them can reveal the health of the forest on a larger scale than field measurements (Sever, et al., 2012). NDVI values range from -1 to +1, where negative values usually indicate open water sources, around 0 indicate urban areas, and values closer to +1 show dense green leaves (Sever, et al., 2012; GISGeography, 2022). NDVI as dNDVI depends on the vegetation type, as different vegetation reflects light in the NIR region. One problem with using space-borne imagery to calculate NDVI is the atmospheric noise from dust, aerosols, and clouds, which can cause negative bias (Beck, et al., 2007). The atmospheric noise distorts the radiance path causing higher reflectance in the red region and a decreased reflectance in the NIR region (Beck, et al., 2007). Another problem with NDVI is soil interference, where high soil moisture or low vegetation cover will result in higher reflectance in the visible spectra, causing a lower NDVI.

dNDVI, similar to dNBR, is used to map out changes to vegetation (McKenna, et al., 2018). dNDVI uses images from previous years and following years to identify vegetation regrowth after a disturbance event.

4. Methodology

The project was divided into two main areas: RS processing and fieldwork. The objective of this report, as stated in the aim, is to investigate how well satellite imagery performs on large-scale assessment of fire damage and forest health, as well as performance correlation to field sampling. The RS processing was carried out at the beginning of the project, and the fieldwork was carried out later. Site selection is the same for both parts but differs in collection and processing.

4.1. Site selection

The study area of interest is based on previous field measurement sites from Johan Eckdahl (Eckdahl, et al., 2022). As the study was carried out in the spring of 2022, burned sites located on the southeast coast of Sweden were chosen to investigate (Figure 2). One additional site in Värmland county was also selected to study based on

the previous knowledge of the area and interest. Each dot in figure 2 represents both the burned site and the corresponding control site.

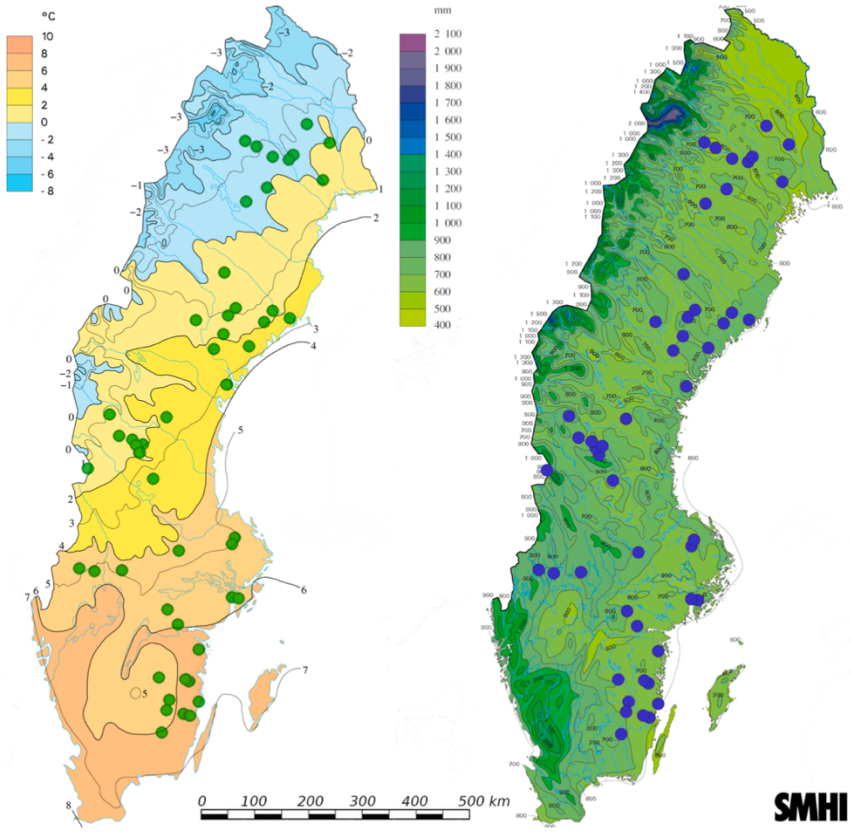

Figure 2. Johan Eckdahls' field sites show Sweden divided in gradients based on SMHI's climate data between 1961 and 2017. The first map shows temperature gradients, and the second shows rainfall in mm. The figure is taken from Eckdahl and colleges (Eckdahl, et al., 2022).

For the site selection, some criteria were put into place. The first criterion was to filter out sites that still face frozen precipitation (snow or hail) or have multiple frost nights (nights below 0 ºC) in May. This is due to complications of tree core sampling as trees do not retain water during the winter months, and thus the samples might crumble. The second criterion was that the sites had to have available satellite data for pre-fire (2017), post-fire (2019), and the following years leading up to 2021. The last criterion for site selection was to identify if any sites have been clear-cut since 2019. This was done by checking satellite images in google earth pro (Google Earth, 2022).

4.1.2. Site description

The sites used in this study were located in the boreonemoral zone (Figures 1 and 2). The site was dominated by pine plantation forests grown on well-drained podzol soil. All sites were located in no permafrost zones. For the burned and control plots, the understory vegetation was dominated by different kinds of moss, blueberry shrubs,

grass, and occasionally lingonberry shrubs. No canopy fires were present in the burned plots, but different scarring levels were present (Appendix III). Most burned sites contained deadwood in various stages of decomposition except the site Stormandebo (Appendix VIII).

Table 1. Additional site information for all plots used in the study. Age = standing age of the forest, Bare_rock = visual estimate of the percentage of bare rock, Plant_cover = visual estimate of the percentage of plant cover by understory, pH = organic layer pH, Mortality = visual estimate of the percentage of dead trees, CHAR = kg/m/m of char on the top layer of the soil, C = kg/m/m of C in the organic layer, Moisture = raster data for soil drainage (unitless), and SPEI = SPEI drought index. Additional information was provided by Eckdahl and colleagues (2022).

Area	Plot ID	Age	Bare_Rock	Plant_cover	pH	Mortality	CHAR	C	Moisture	SPEI
Kil	71	63	2	0	3.4	52.94	1.43	4.82	57.56	-1.49
Kil	72	63	1	99	4.05	0	0	3.11	26.16	-1.49
Österbymo	81	82	20	5	3.79	59.37	1.51	4.98	51.71	-2.07
Österbymo	82	78	5	95	3.77	3.12	0	3.88	69.25	-2.07
Rullerum	83	62	10	2	3.84	16.66	1.39	2.22	7.10	-2.02
Rullerum	84	31	20	80	3.91	15.38	0	5.51	8.10	-2.02
Stormandebo	85	71	5	0	3.76	30	3.47	3.15	17.14	-2.02
Stormandebo	86	99	20	80	3.54	22.72	0	3.17	26.50	-2.02
Lessebo	99	88	40	0	4.16	98.07	2.48	3.85	65.42	-1.81
Lessebo	100	76	0	100	3.4	0	0	9.31	105.50	-1.81

4.2. Data collection

4.2.1. Satellite data

Satellite data was collected using GEE (GEE, 2022) to assess satellite performance. GEE is a geoportal allowing users to view, process, analyse, and download geospatial data for academic or research purposes for free (GEE, 2022). The software will enable users to download data from the satellites: Sentinel-2, MODIS, GRACE, Landsat, etc. (GEE, 2022). The satellite data used in this study was the Sentinel-2 Copernicus twin satellite Level-2A orthorectified atmospherically corrected surface reflectance (ESA, 2022). This allows users to assess 10m spatial resolution easily compared to other satellites with a lower spatial resolution.

The burn sites and control plots point coordinates were converted to rectangle coordinates to cover roughly a 3 km-by-1.5 km area. The large area helps distinguish the forest from lakes, urban areas, and agriculture but also captures the entire burn site and the control plots in the same image. The burn sites were cross-referenced from Skogsstyrelsens burn polygons to ensure that the site covers the entire burn site (Skogsstyrelsen, 2022). The conversion from point coordinates to rectangles was made in the programming software MATLAB (MatLab, n.d.). This conversion can be seen in Appendix I.

Before downloading the data and processing them, several filters were applied. The first filter applied was the start date and end date. The start date was May 1st, 2018, as the fires mainly occurred from the end of June to the beginning of August during the drought season in Sweden (SMHI, 2019). The end date was September 1st, as most fires had already stopped or were mostly smoulder fires where the damage could already be seen. The start and end dates were applied to all years from 2017 to 2021. Each year's tree increment pattern correlates to the vegetation season's growth. Thus, the satellite data were extracted for these months to accurately represent the increment patterns.

A cloud cover filter was also applied to filter out images with more than 100 % cloud cover. In ideal situations, images with zero cloud cover are of interest, but the photos taken containing the interest area could have cloud cover that might not be seen in the interest area and thus be filtered away. The GEE code for downloading can be seen in Appendix II. A MATLAB code for discarding unwanted photos was used to ensure the images were of high quality and did not contain any cloud shadows or clouds covering the direct site. This code was written by Veiko Lehsten and can be seen in Appendix III.

4.2.2. Field samples

The field sites for coring were divided into five sites, containing a burn plot and a corresponding control plot located around < 100 m away from the burned plot (Table 1). Four sites were located in southern Sweden and one in Värmland county.

The tree cores were extracted using an increment borer (5.15 mm Ø) following the user manual (Haglöf Sweden, 2022). The cores were drilled at the height of 1.4 m – 1.5 m (chest height) and on the sides of the trees with minimal to no burn scars. Trees with a Ø > 25 cm were cored to ensure that a minimum of 30 years was captured in the core. 4 - 5 trees were cored twice, providing 8 – 10 cores per plot (Table 1, Appendix IV). Cores were taken from *Pinus sylvestris* trees with partial to intact crowns. Additionally, dead *Pinus sylvestris* trees with burn scars were cored as well (Appendix IV).

Table 2. Table showing area for the burn plots and control, with their corresponding coordinates. The table also shows tree sp. and the total number of trees cored for each site.

Burned plots

Area	Plot	Long	Lat	Tree sp.	Trees cored
Kil	71	13.248167	59.597367	Pinus Sylvestris	5
Österbymo	83	15.35082	57.80882	Pinus Sylvestris	5
Rullerum	81	16.617233	58.26775	Pinus Sylvestris	5
Stormandebo	85	16.3014998	57.7467978	Pinus Sylvestris	5
Lessebo	99	15.43149	56.8721	Pinus Sylvestris	4

Control plots

Area	Plot	Long	Lat	Tree sp.	Trees cored
Kil	72	13.249433	59.596633	Pinus Sylvestris	5
Österbymo	84	15.350241	57.808176	Pinus Sylvestris	5
Rullerum	82	16.617467	58.2668	Pinus Sylvestris	5
Stormandebo	86	16.30155	57.747101	Pinus Sylvestris	5
Lessebo	100	15.42874	56.87192	Pinus Sylvestris	5

4.3. Data processing

4.3.1. Remote sensing processing

Data processing for satellite data used the programming software MATLAB (MatLab, n.d). The following calculations have been converted into a MATLAB code that automatically calculates the NBR, NDVI, dNBR, and dNDVI for all sites (Appendix V).

4.3.1.1. Fire Damage Severity

Fire severity and damage were determined by using dNBR. dNBR is used to assess burn severity after a fire event, where the severity is estimated using RS data pre-fire and postfire events. RS data from 2017 was used as pre-fire indices and 2019 as postfire indices for the different sites and was calculated as follows:

$$\mathrm{NBR} = \frac{NIR - SWIR}{NIR + SWIR}$$

$$dNBR = NBR_{(pre-fire)} - NBR_{(post-fire)}$$

where *NIR* is the near-infrared band, and *SWIR* is the shortwave infrared band (Holden, et al., 2016; Bäckström & Grenert, 2019). The dNBR is later calculated using the prefire values and the postfire values, where high values (dNBR > 0.8) correspond to high fire severity (Quintano, et al., 2018). Both NBR and dNBR are unitless indices.

4.3.1.2. Forest Health Estimation

Vegetation health and regrowth can be assessed using NDVI. NDVI measures the "greenness" (chlorophyll) of healthy vegetation by looking into the reflectance band for vegetation (NIR) and the absorbent band (Red) (Lange, et al., 2017; GISGeography, 2021). The healthy vegetation reflects more in the NIR spectral wavelengths. Thus, having a higher value (close to +1), less healthy vegetation will reflect at lower levels (NDVI < +0.5). NDVI was calculated as follows:

$$\text{NDVI} = \frac{NIR - Red}{NIR + Red}$$

$$dNDVI = NDVI_{(Pre-fire)} - NDVI_{(Post-fire)}$$

where *NIR* is the near-infrared spectral band, and *Red* is the red band (Sunar & Özkan, 2001). The dNDVI was calculated using NDVI values pre-fire (2017) and postfire (2018). Both NDVI and dNDVI are unitless.

4.3.2. Tree-ring processing

The tree rings were processed following the standard dendrochronology procedures (Bräker, 2002; Edvardsson, et al., 2019). The cores were wetted and shaved to expose the cellular structures of the rings. Following the preparation of the cores, the cores were dried at room temperature for 3 - 24h before measurement. The tree rings were measured to the nearest 0.01 mm using the digital LINTAB positioning table connected to a Leica stereomicroscope and TSAPWin Scientific software (Rinn, 2022a; Rinn, 2022b; Leica, 2022; Edvardsson, et al., 2019). TSAPWin allows users to measure and analyse tree rings and can be applied to different scientific fields (Rinn, 2003). All equipment and software were used following the user manual. The cores were given specific core IDs in the TSAPWin program to be stored in the database (Appendix IV).

The measured rings were then processed using the software ARSTAN_44xp following the user manual (Cook & Holmes, 1999). The program minimises the influences of non-climatic variations, ultimately transforming the ring's width into dimensionless indices (ARSTAN indices) that are unitless (Cook & Holmes, 1999; Edvardsson, et al., 2019).

4.4. Data analysis

As this report is a pilot study for a more extensive project, the study was only conducted for a smaller sample size. Thus, the results are based on this sample size. Some analyses could not be carried out but are presented in the following section and explained further.

4.4.1. Visualization of burn severity and forest health signal

The reflectance values were transformed and categorised to validate if the fire signal is strong enough to be captured using satellite burn severity estimation (Appendix V). The different categories included: high severity (reflectance ≥ 0.6), moderate severity (0.6 > reflectance ≥ 0.4), low severity (0.4 > reflectance ≥ 0.2), and unburnt (reflectance < 0.2). The categorisation thresholds were established by looking at the frequency distribution of the reflectance values.

For estimation of forest health, the reflectance values, like dNBR, was transformed and categorized into four robust categories (Appendix V): no regrowth (reflectance ≥ 0.3), low regrowth (0.3 > reflectance ≥ 0.2), moderate regrowth (0.2 > reflectance ≥ 0), and regrowth detected (reflectance < 0). To estimate vegetation loss for each site, the dNDVI was derived using pre-fire vegetation reflectance (end of 2017) and post-fire vegetation reflectance (end of 2018). To visualise the health of the forest after the fire disturbance in 2018, NDVI reflectance for 2021 was used as a post-fire for dNDVI assessment.

4.4.2. Validation of RS methodology and forest increment patterns

To be able to validate if using RS methodology is a viable tool for estimating burn severity and forest recovery in Fennoscandia, different statistical tests were performed. For each site, the dNBR and NDVI values were extracted for analysis by taking the surrounding pixel values for the burned and control plot. The median pixel value corresponds to the coordinates for each plot. The nine pixels were then averaged to create one value for analysis (Appendix V).

To establish that the fire disturbance of 2018 influenced the boreal forests' growth patterns, the mean value and standard deviation (SD) were derived by using the ARSTAN indices between 2010 - 2017 as the pre-fire growth ratio. The ratio was then established for 2018, 2019, 2020, and 2021 by dividing the yearly value by the pre-fire growth indices. The following year's mean value and SD were then determined for the control and burned plots.

The growth indices for each year were then tested for differences in significance ($p < 0.05$) by taking the burned and control plot against each other to verify if there is any difference between them.

Due to the small sample size and unequal distribution, a permutation test was done using the add-on function provided in MATLAB (Krol, 2021) (Appendix VI). A

permutation test is built on the assumption that there is no difference in means between the two populations and is another form of hypothesis testing. The permutation test assumes that the two populations are independent of each other and looks into the means of the population groups, similar to bootstrap techniques. The function returns a p-value, and if the p-value is below the significance threshold ($p < 0.05$), the null hypothesis is rejected. The permutation test also returns the effect size (Hedges 'g), which determines the actual difference in means between the two groups. Hedges' g effect size tells how much the two population differs from one another. An effect size of ≥ 0.8 is determined as a large effect and thus can be seen by the naked eye, an effect size of below < 0.2 is considered trivial. The null hypothesis for permutation states:

H_0 = The samples come from the same mean distribution.

This test was performed to establish if there are any differences in the satellite imaging and ARSTAN indices between control plots and burned plots.

The tests were also conducted to see if there is any significance between the pre-fire state (average indices 2010 to 2017) and post-fire (2019) for ARSTAN growth indices. For dNBR, the tests were run in the same manner as seen above between control and burned plots, but for NDVI, this was done for all years and between pre-fire and post-fire, like the indices. The burn and control plots value for the dNBR and NDVI was estimated by taking the mean value of the surrounding pixels.

To establish if there is any correlation between the RS methodology (burn severity and NDVI) with growth indices, an R^2 (correlation coefficient) value, Spearman's rank correlation coefficient, and root-mean-square-error (RMSE) would be conducted. In this report, a visual scatter correlation was conducted between dNBR and ARSTAN indices, and a time-series visual correlation was determined for NDVI and ARSTAN indices for the years 2017-2021. This is due to the small sample size, as the intended correlations can be regarded as to biased and not representative of the boreonemoral wildfires in Sweden. Thus, no statistical analysis was conducted for the correlation coefficient in this report.

4.5. Funding

All travel expenses such as car, hotel, and equipment were funded by the BECC's project: *Learning from a fire prone past for a fire prone future: Assessing the effect of forest fires (pilot project)*. Lab equipment and program licenses were provided by Lund University.

5. Result

5.1. Analysis of fire disturbance signal for the study areas

The fire signal can be visually distinguished for medium to larger fires (Figures 3, 4, and 7). Burn severity categorization for the largest sites shows a clear low severity

border followed by a moderate severity middle where few pixel values show high severity (Figures 3 and 7). For the medium-sized burn sites, the categorisations show a clear low severity border followed by a moderate severity middle (Figures 4 and 5). The most minor fire site (Figure 6) shows a weak signal in the low categorisation with very few pixels in the moderate severity classification outside the sampling point. The sampling point for Stormandebo (Figure 6) shows unburnt values where the sampling has been done, indicating that the fire signal (dNBR values) is too weak to be picked up by the satellite instruments. The dNBR values for both categorised and uncategorized indices also show disturbance signals outside of the sites.

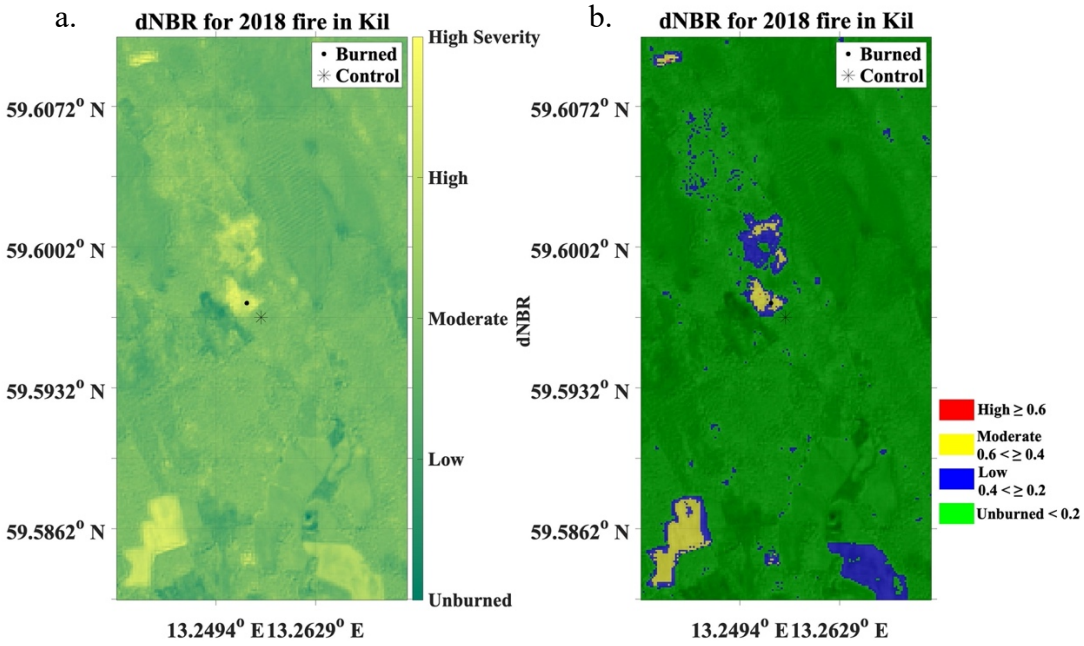

Figure 3. Map of the study area Kil. Dot (.) = Burn site, and Star (*) = Corresponding control site. A) shows the raw dNBR index values ranging from unburnt (dark green) to high severity (bright yellow). B) shows the categorized dNBR index values classified into: High severity ≥ 0.6, Moderate severity 0.6 < ≥ 0.4, Low severity 0.4 < ≥ 0.2, and Unburnt < 0.2.

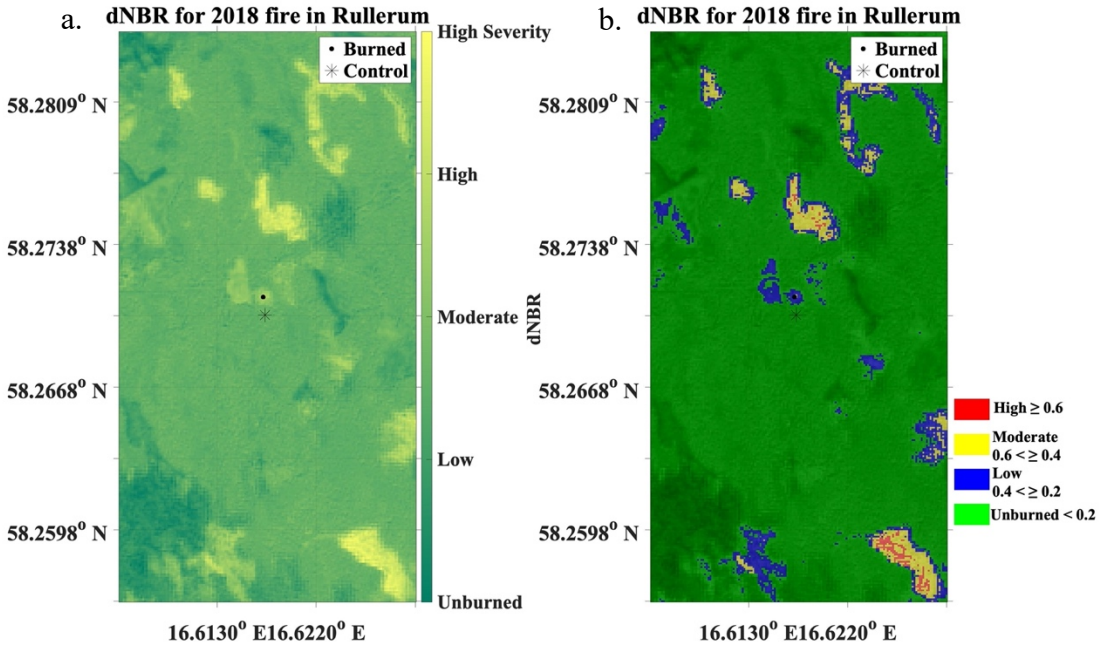

Figure 4. Map of the study area Rullerum. Dot (.) = Burn site, and Star (*) = Corresponding control site. A) shows the raw dNBR index values ranging from unburnt (dark green) to high severity (bright yellow). B) shows the categorized dNBR index values classified into: High severity ≥ 0.6, Moderate severity 0.6 < ≥ 0.4, Low severity 0.4 < ≥ 0.2, and Unburnt < 0.2.

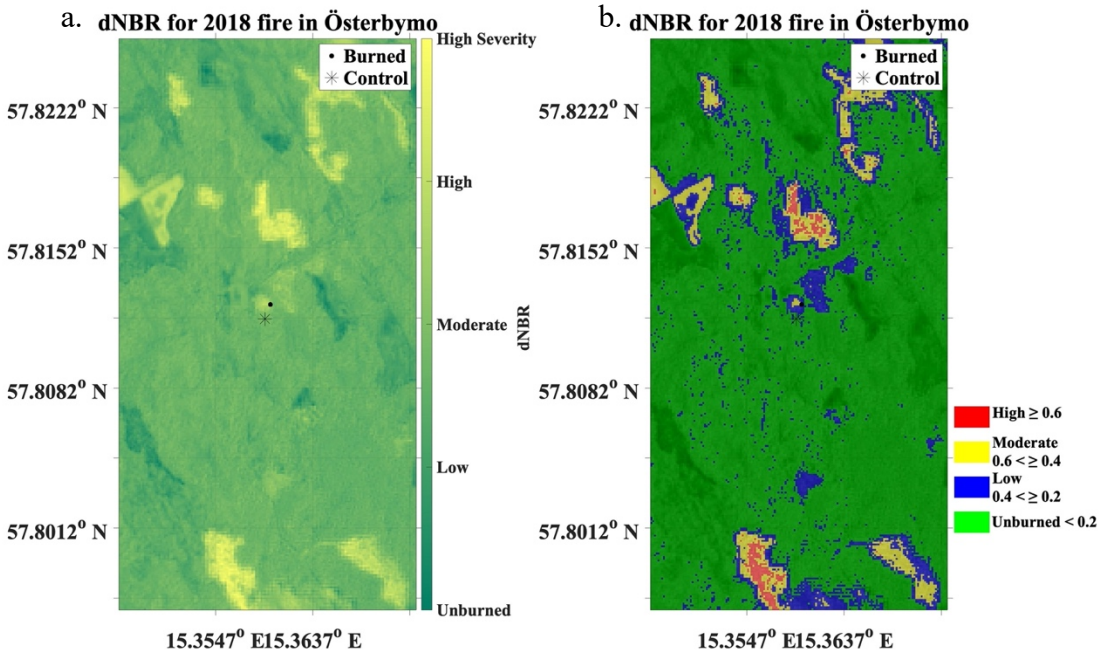

Figure 5. Map of the study area Österbymo. Dot (.) = Burn site, and Star (*) = Corresponding control site. A) shows the raw dNBR index values ranging from unburnt (dark green) to high severity (bright yellow). B) shows the categorized dNBR index values classified into: High severity ≥ 0.6, Moderate severity 0.6 < ≥ 0.4, Low severity 0.4 < ≥ 0.2, and Unburnt < 0.2.

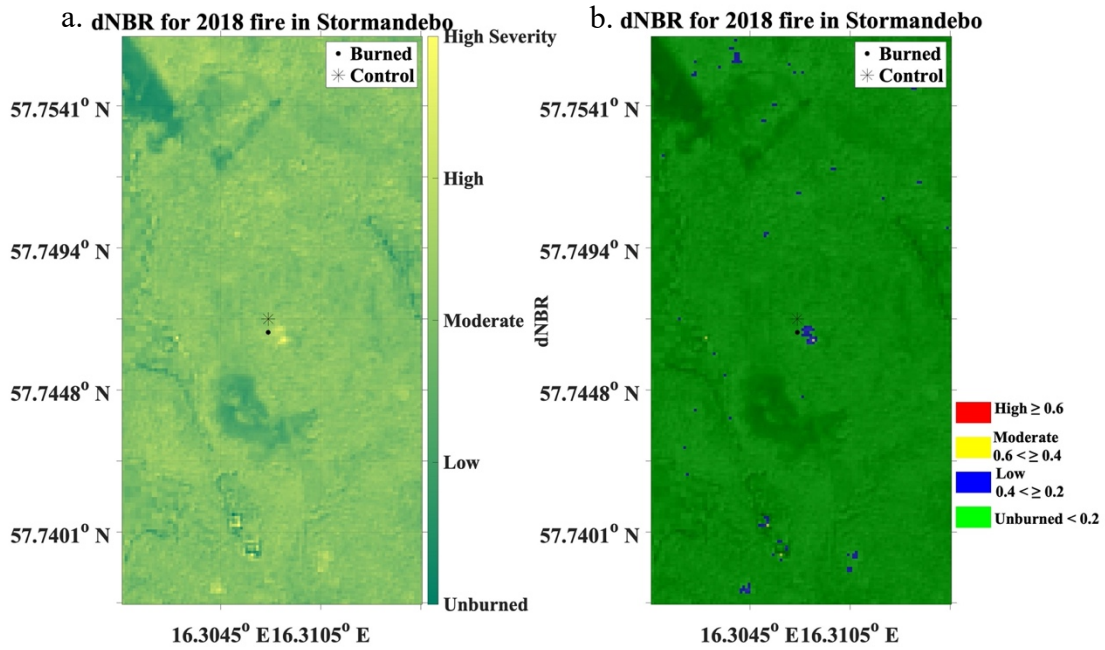

Figure 6. Map of the study area Stormandebo. Dot (.) = Burn site, and Star (*) = Corresponding control site. A) shows the raw dNBR index values ranging from unburnt (dark green) to high severity (bright yellow). B) shows the categorized dNBR index values classified into: High severity ≥ 0.6, Moderate severity 0.6 < ≥ 0.4, Low severity 0.4 < ≥ 0.2, and Unburnt < 0.2.

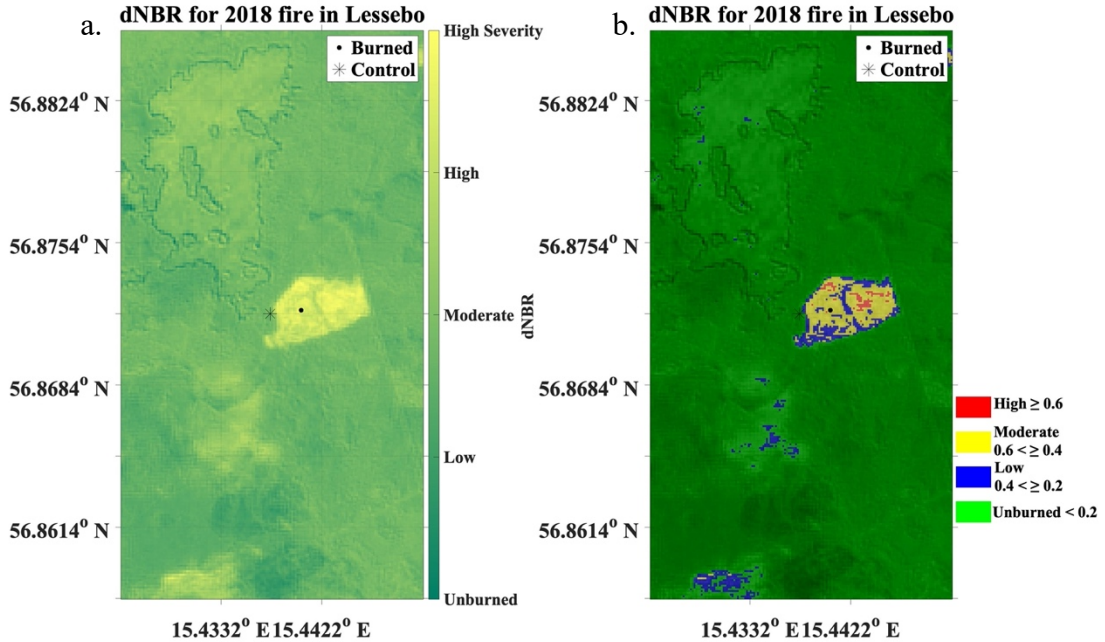

Figure 7. Map of the study area Lessebo. Dot (.) = Burn site, and Star (*) = Corresponding control site. A) shows the raw dNBR index values ranging from unburnt (dark green) to high severity (bright yellow). B) shows the categorized dNBR index values classified into: High severity ≥ 0.6, Moderate severity 0.6 < ≥ 0.4, Low severity 0.4 < ≥ 0.2, and Unburnt < 0.2.

5.2. Burn severity's impact on tree ring width for control and fire-affected areas

The analysis of the ARSTAN indices was tested between the plots for each year. The ARSTAN growth indices show a decrease in the mean between 2017 to 2018, with a value of 0.366 for the control plot. A similar trend of decline (decrease of 0,287) can also be detected for the burned plot, however not as large as the control (Table 3). Decrease of the mean value continues for the burned plot, where the decrease in indices is at the lowest 2019 (mean value of 0,686), one year after the fire disturbance. The control plot shows a faster recovery than the burned plot by looking at the mean ARSTAN indices value. The control and burn plots show an increase in growth following the decrease, but they do not reach the same mean value as pre-fire (mean 2010-2017).

The variance for control and burn plots shows low variance (< 0.1), indicating that the values are close to the mean with slight variance between the sample and its mean value (Table 3). However, for the burned plot, the variance is slightly higher for the year 2018 and 2019, showing a somewhat larger spread of the data points. The permutation test indicates no difference between the ARSTAN indices for control and burned. Thus, concluding no statistical difference between them as the p-value was over the threshold. This is also shown in Hedges' g, where the effect size is below the point to be considered "medium effect", meaning that the two plots are similar.

Table 3. Table of the statistical analysis for ARSTAN growth indices values for burned and control plots (unitless). The tests were conducted year-wise. The table shows the mean value with their corresponding standard deviation (SD) values, Hedges 'g (unitless), and permutation test for equal means.

	Mean ± SD		Permutation test		Sample size
	Control	Burned	Significance ($p \leq 0.05$)	Effect size (Hedges ' g)	
	ARSTAN indices comparison between control and burned sites				
Average 2010-2017	1,064 ± 0,082	1,087 ± 0,082	0,655	0,27	5
2018	0,698 ± 0,169	0,8 ± 0,365	0,578	0,36	5
2019	0,885 ± 0,094	0,686 ± 0,33	0,249	-0,82	5
2020	0,973 ± 0,245	0,739 ± 0,162	0,109	-1,12	5
2021	0,952 ± 0,128	0,824 ± 0,193	0,304	-0,78	5

The analysis of the dNBR mean values is disclosed in Table 4 and shows a difference in means between the burn and control plots (difference of 0,254). The difference between the control and true middle of the burn plots shows a higher difference (difference of 0,345), indicating that the burned plot middle value has a higher dNBR than the field sample burn plot. This can also be observed when comparing the dNBR values between the sample burn plot and true middle burn values (difference of 0.091).

Each dNBR plot shows a low variance for the variance, indicating that the dNBR values do not vary excessively from the mean value.

The permutation test revealed a statistically significant difference between the control dNBR values and two different dNBR burn values (Table 4). The p-value for control dNBR and burned dNBR values (field sampling burn plot) shows a value of 0.019 with an effect size (Hedges' g) of 1.79. This indicates that the difference between the control dNBR and burned dNBR mean values is statistically significant. The p-value between the control dNBR and the burned plot true middle dNBR value shows a value of 0.025, with an effect size of 2.15. The higher effect size indicates a more significant difference between the values and their means compared to the control and field sampling burn plot but statistically shows a lower p-value. No difference was found between the burn plots dNBR values and the true middle dNBR values.

Table 4 shows a low spread of the mean pixel values for the control dNBR values, ranging from 0 to 0.1 (unburnt values). For the dNBR, the field sampling burn plot values range from 0.1 to ≈ 0.4 (unburnt to moderate severity), while the true burn middle values range from ≈ 0.25 to ≈ 0.55 (low severity to moderate severity). This indicates that the true middle burn plot shows a wider spread in the different severity classes whilst the field burn sample values range mainly in the low severity to unburnt and touch moderate severity.

Table 4. Table of the statistical analysis for dNBR values (unitless) for the burned, middle of the burned plot (true middle), and control plots. The table shows the mean value with their corresponding standard deviation (SD) values, Hedges 'g (unitless), and permutation test for equal means.

	Mean ± SD		Permutation test		Sample size
	Control	Sample	Significance ($p \leq 0.05$)	Effect size (Hedges ' g)	
	dNBR comparison control vs. Burned (Sample)				
dNBR Control vs. Burned (sample)	0,037 ± 0,065	0,291 ± 0,189	**0,019**	**1,79**	5
dNBR Control vs. True middle (sample)	0,037 ± 0,065	0,382 ± 0,217	**0,025**	**2,15**	5
dNBR Burned (control) vs. True	0,291 ± 0,189	0,382 ± 0,217	0,478	0,45	5

By analysing the relationship between dNBR (control and burned) and ARSTAN indices for 2019, no clear visible correlation could be observed (Figure 8). Under normal circumstances, a correlation coefficient analysis would be performed to investigate further if a correlation can be established. The control values show a higher growth increment with a corresponding low dNBR value, except for the site Lessebo that have a high dNBR value and high growth increment. Most of the dNBR values were found to have a correlating growth increment between 0.3 – 0.75.

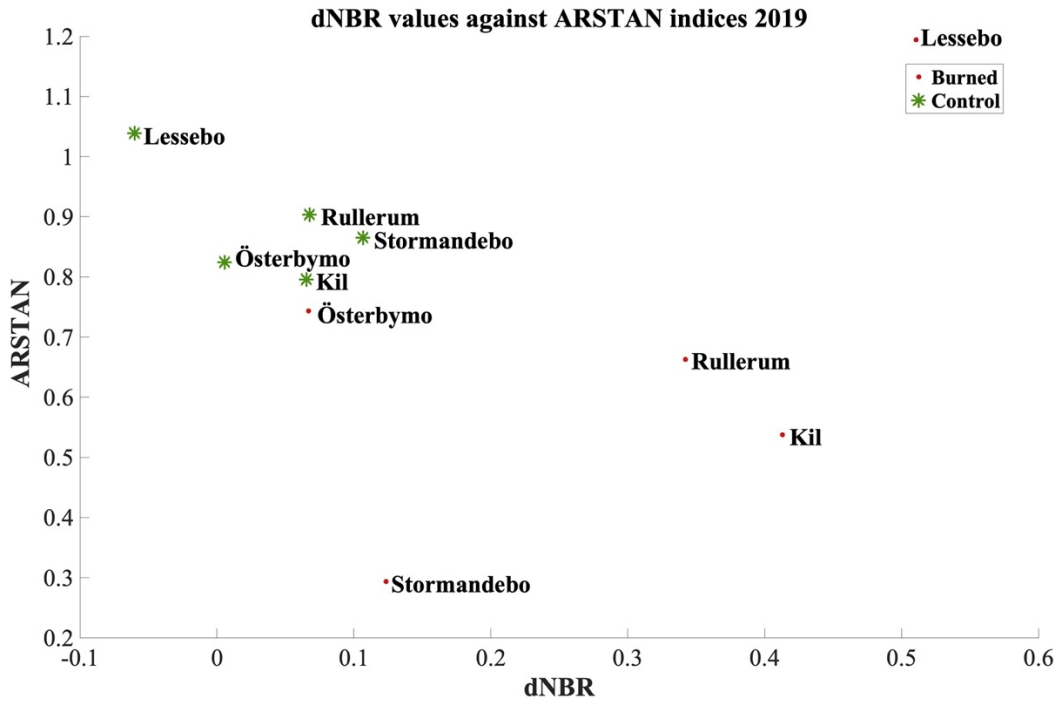

Figure 8. Scatterplot showing ARSTAN growth frequencies for 2019 and the corresponding dNBR values for the control and burn sample site. Y-axis shows the ARSTAN growth frequencies, and the x-axis shows the dNBR value. Burned = red dot (.) and Control = green star (*). All sites have been marked with their corresponding name.

5.3. Analysis of forest health after a fire disturbance for control and fire-affected areas

Analysing the visualization of the dNDVI signal between the fire year (2018) and pre-fire (2017), most fire damages can be distinguished. In the sites Kil and Rullerum (Figure 9a and 10a, respectively), the fire damage signal can be easily distinguishable between the fire year (2018) and pre-fire year (2017). Kil (Figure 9a) shows even a larger area of vegetation loss compared to the dNBR for the site (Figure 3a). However, for the sites Rullerum and Stormandebo, the fire damage and burn severity perimeter is visually different (Figures 4a and 9a for Rullerum, and Figures 6a and 12a for Stormandebo). The vegetation loss perimeter where the fire disturbance occurred could not be distinguishable for the sites Österbymo and Lessebo (Figures 11a and 13a).

Throughout the image, there is an apparent reduction of vegetation between the years 2017 and 2018, indicating an overall disturbance occurred between the years. The pixel categorisation was classified as moderate regrowth; thus, the disturbance was not too severe to damage the surrounding area to a point where no vegetation was detected.

Analysing the vegetation regeneration between 2017 and 2021 for dNDVI shows that most sites have a positive regeneration compared to the dNDVI values between 2017 and 2018 (Figures 9b, 10b, 11b, and 12b). Lessebo (Figure 13b) shows an apparent

reduction in vegetation recovery compared to the other sites. This is of interest as this can indicate secondary disturbance or a fire disturbance that happened later than the 1st of September 2018. Österbymo was the only site showing positive forest regrowth after the fire disturbance, according to the visual analysis (Figure 11b).

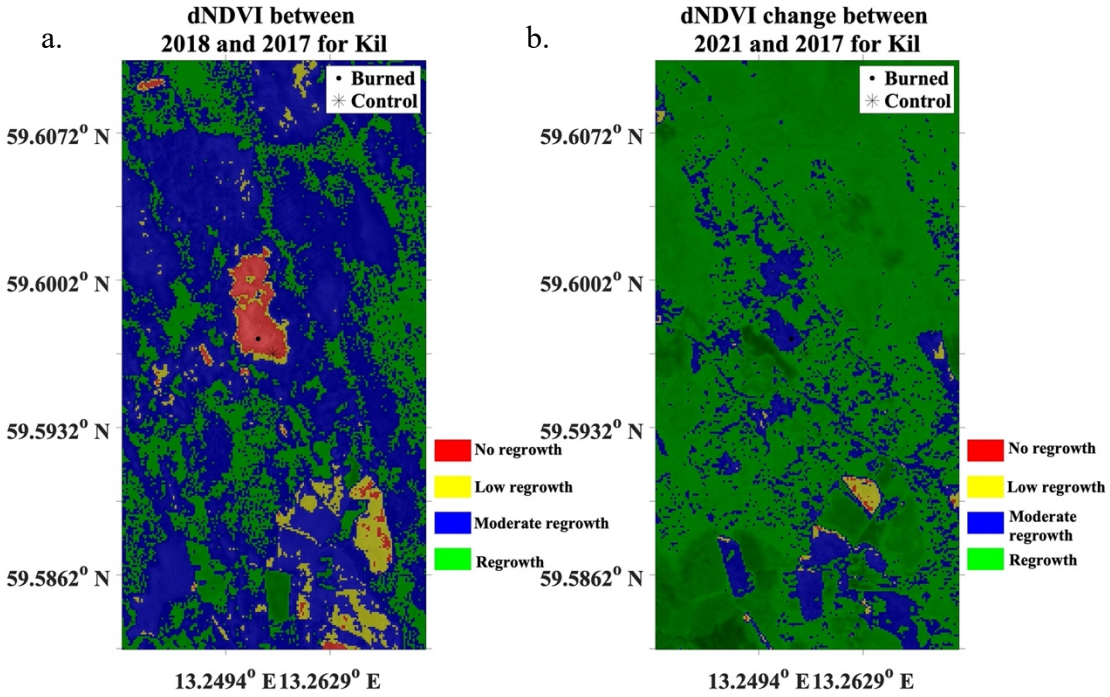

Figure 9. Map of the study area Kil. Dot (.) = Burn site, and Star (*) = Corresponding control site. A) shows the dNDVI index values from 2017 and 2018. B) shows the dNDVI index values from 2017 and 2021. dNDVI index values classified into: No regrowth ≥ 0.3, Low regrowth $0.3 < \geq 0.2$, Moderate regrowth $0.2 < \geq 0$, and Regrowth < 0.

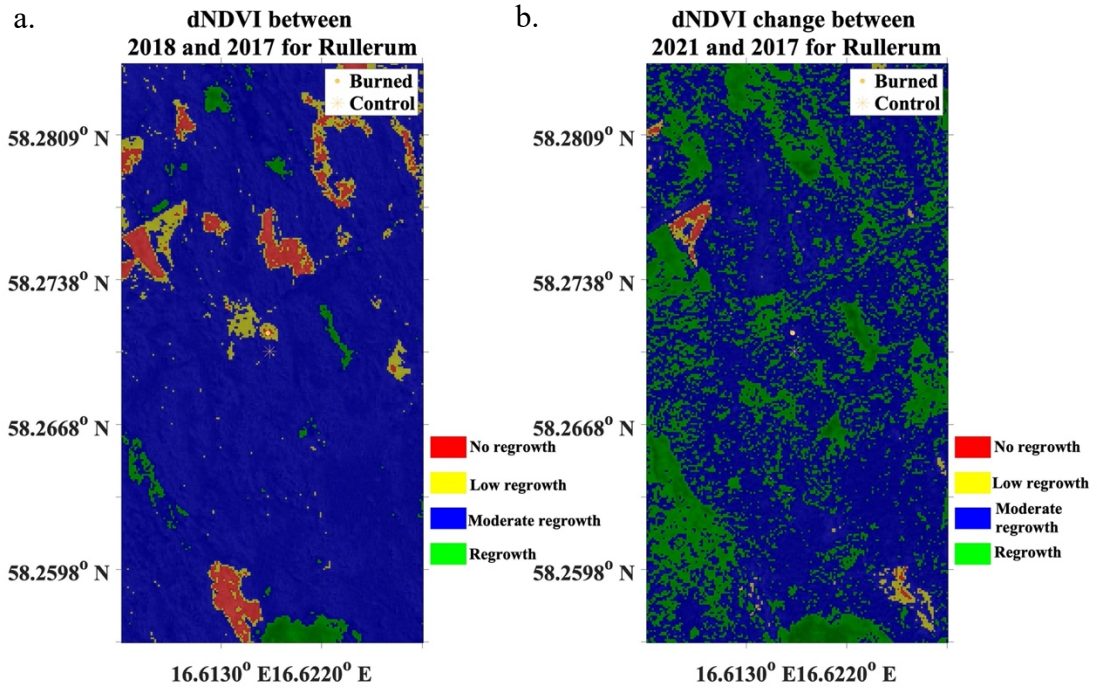

Figure 10. Map of the study area Rullerum. Dot (.) = Burn site, and Star (*) = Corresponding control site. A) shows the dNDVI index values from 2017 and 2018. B) shows the dNDVI index values from 2017 and 2021. dNDVI index values classified into: No regrowth ≥ 0.3, Low regrowth 0.3 < ≥ 0.2, Moderate regrowth 0.2 < ≥ 0, and Regrowth < 0.

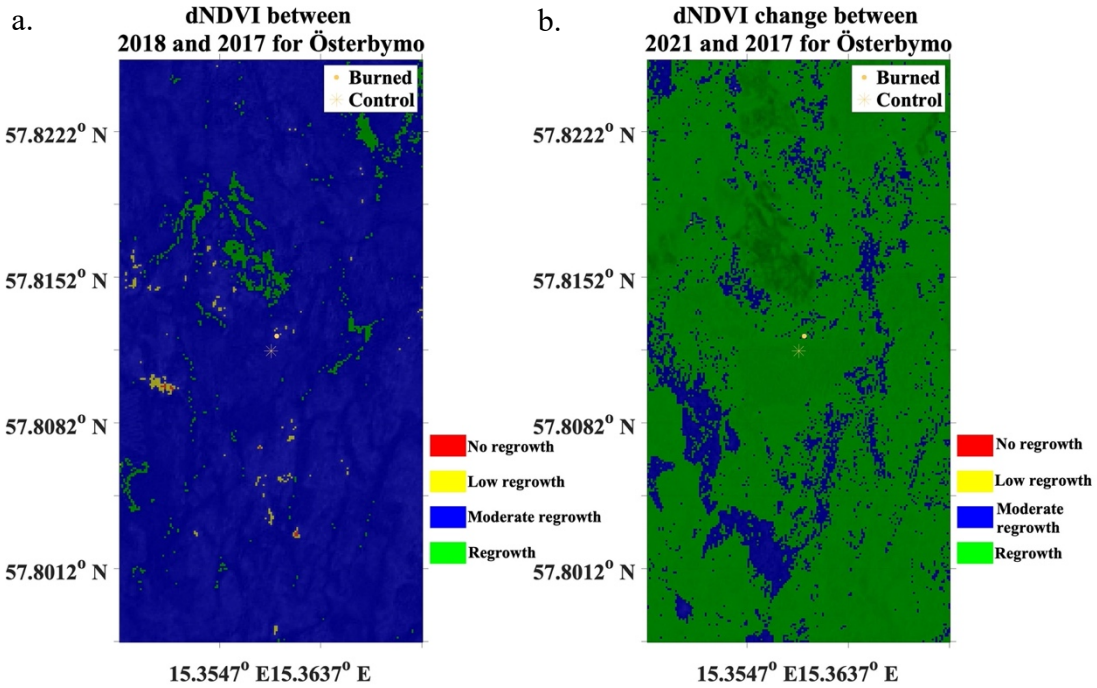

Figure 11. Map of the study area Österbymo. Dot (.) = Burn site, and Star (*) = Corresponding control site. A) shows the dNDVI index values from 2017 and 2021. B) shows the dNDVI index values from 2017 and 2021. dNDVI index values classified into: No regrowth ≥ 0.3, Low regrowth 0.3 < ≥ 0.2, Moderate regrowth 0.2 < ≥ 0, and Regrowth < 0.

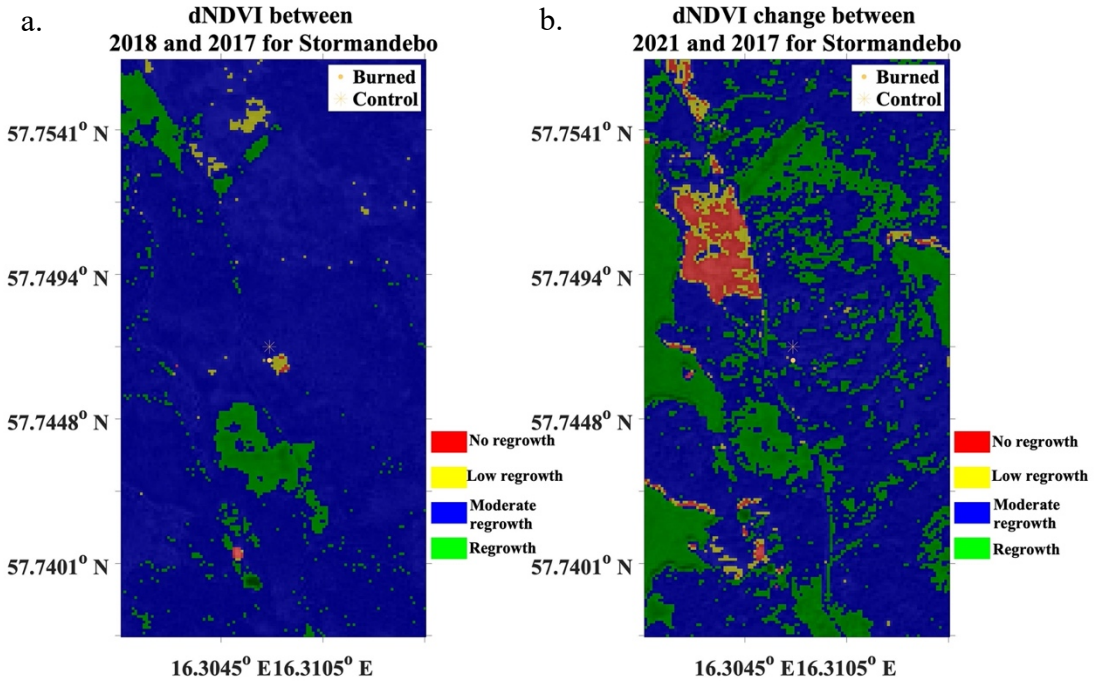

Figure 12. Map of the study area Stormandebo. Dot (.) = Burn site, and Star (*) = Corresponding control site. A) shows the dNDVI index values from 2017 and 2018. B) shows the dNDVI index values from 2017 and 2021. dNDVI index values classified into: No regrowth ≥ 0.3, Low regrowth 0.3 < ≥ 0.2, Moderate regrowth 0.2 < ≥ 0, and Regrowth < 0.

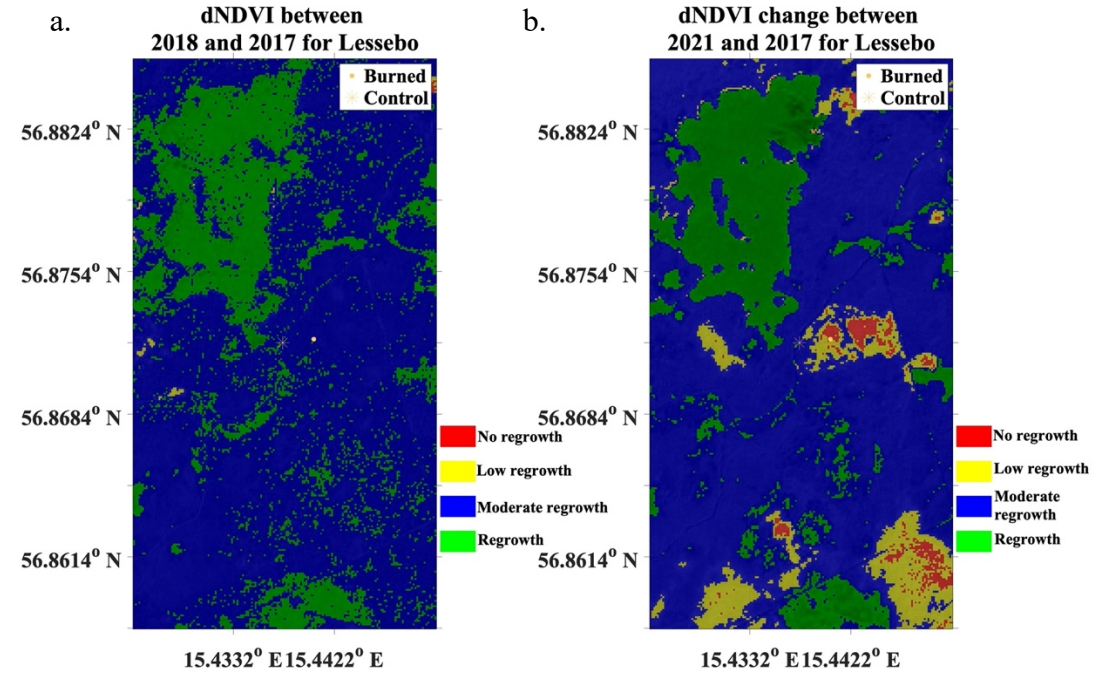

Figure 13. Map of the study area Lessebo. Dot (.) = Burn site, and Star (*) = Corresponding control site. A) shows the dNDVI index values from 2017 and 2018. B) shows the dNDVI index values from 2017 and 2021. dNDVI index values classified into: No regrowth ≥ 0.3, Low regrowth 0.3 < ≥ 0.2, Moderate regrowth 0.2 < ≥ 0, and Regrowth < 0.

5.4. Vegetation growth with NDVI and tree ring width

Analysing the differences in mean values for NDVI between 2017 and 2021 for the control area shows an increase in NDVI for 2019 (Table 5). This increase of 0,046 from the overall mean of ≈ 0.464 is only present in the control area and is only present for 2019. For the burn area, the mean value starts to decrease in 2018 and continues to decline until 2021, when a slight increase of ≈ 0.026 can be detected. This indicates that the control area shows a relatively stable NDVI where the burn area is affected by the 2018 fire disturbance according to the mean NDVI values.

The variance for control and burn plots shows low variance (< 1), indicating that the values are close to the mean value (Table 5). For the permutation test, the only year that showed a statistically significant difference in means was the year 2019, where the p-value was 0.04. This stipulates that a detectable difference can be made one-year post-fire between the values.

Table 5. Table showing the statistical analysis for NDVI values (unitless) between the years 2017 to 2021 for control and burn plots. The table shows the mean value with their corresponding standard deviation (SD) values, Hedges' g (unitless), and permutation test for equal means.

	Mean ± SD		Permutation test		Sample size
	Control	Burned	Significance (p ≤ 0.05)	Effect size (Hedges ' g)	
	NDVI comparison within the same year				
NDVI 2017	0,499 ± 0,047	0,523 ± 0,050	0,47	0,48	5
NDVI 2018	0,468 ± 0,077	0,492 ± 0,111	0,688	0,25	5
NDVI 2019	0,51 ± 0,050	0,33 ± 0,148	**0,04**	-1,26	5
NDVI 2020	0,443 ± 0,123	0,32 ± 0,127	0,132	-0,98	5
NDVI 2021	0,449 ± 0,108	0,346 ± 0,106	0,138	-0,95	5

Analysis of the time-series trends in NDVI and ARSTAN growth frequencies showed an overall low correlation between them visually (Figure 14). Similarities between the growth frequencies and NDVI values can be seen in some figures but only for a maximum of 1 - 2 years. For the site Kil (Figure 14a), the NDVI shows a decline from 2018 until 2020 before increasing. The growth increment shows a decline until 2018 for both controls and burned before they divert. The ARSTAN indices for the burned plot continued to decline until 2019 before starting to increase, while the control shows an increase after 2018.

Rullerum shows an increase in growth increment for the burned plot compared to the control between 2017 and 2018 (Figure 14b). The NDVI decreases for both plots between 2017 and 2018; however, the burned plot NDVI continues to decrease until 2019 before increasing like the control values. The growth increment for the burned plot drops in 2019 before drastically increasing the following years to 2021, while the control values have a slighter decrease until 2020 before starting to grow again.

The site Österbymo shows a decrease in growth rate for both the control and burn plot until 2018 before starting to increase up to the year 2020 before decreasing again (Figure 14c). The NDVI trend value shows an increase for both plots until 2018, when the burned plot NDVI values start to decline, and the control increases before decreasing 2019.

For the site Stormandebo (Figure 14d), all variables show a decrease until 2018, where only the burn growth increment continues to decline until 2019 before increasing. The other variables increased between 2018 and 2019, where the NDVI for the control and the burned plot shows similar trend patterns of increasing and later decreasing. The ARSTAN growth indices for the control plot continue to grow at a similar rate after 2019.

The last site (Lessebo) shows similar trends for all variables except the control growth increment for the control plot that declines between 2017 and 2018 (Figure 14e). The NDVI for the burned plot shows a rapid decline after 2018 until 2019 before slowly starting to increase again, where the NDVI for the control plot shows slight variations in the trend. The growth increment for the control plot starts to increase between 2018 and 2020 before decreasing, while the burn growth rate starts to decline in 2019 and continues to decline up to 2021. The ARSTAN growth indices and NDVI control show a similar trend pattern until 2019.

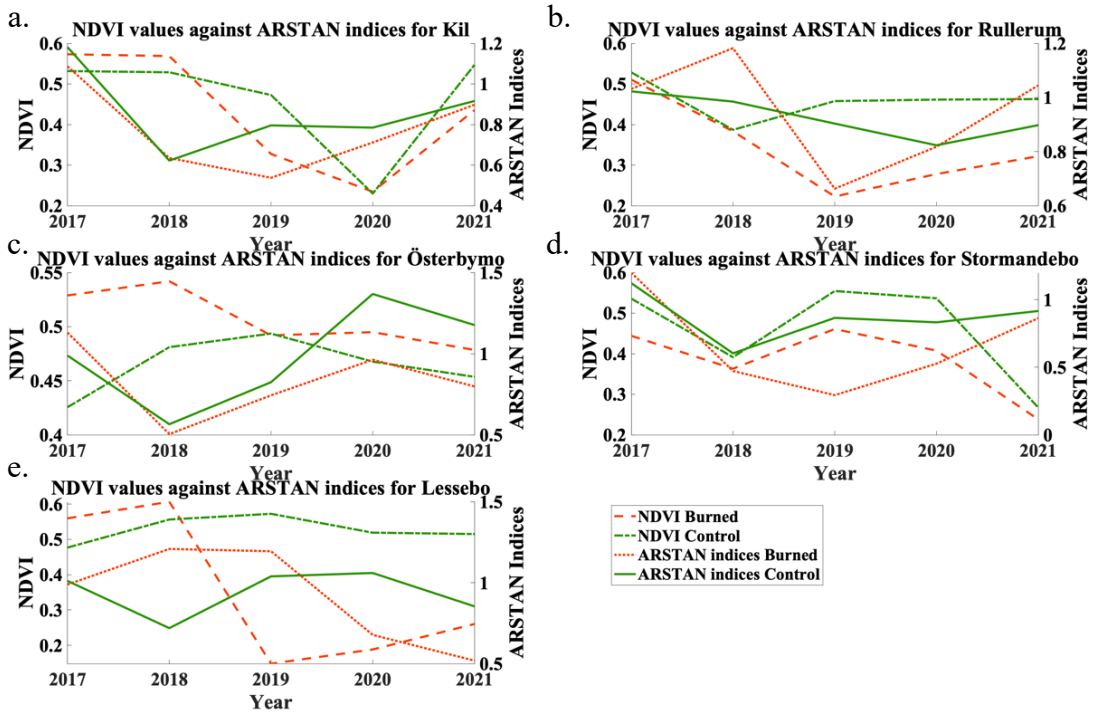

Figure 14. Figure showing temporal changes for NDVI and ARSTAN growth indices between 2017 and 2021 for burned and control plots. The red colour indicates burned, and green indicate control. The different lines correspond to the different variables: NDVI burned (-.), NDVI control (--), ARSTAN indices burned (…), and ARSTAN indices for control (-). Y-axis left shows the NDVI values, the y-axis right shows the

ARSTAN growth indices, and the x-axis shows the year. The sites shown in the figure are A) Kil, B) Rullerum, C) Österbymo, D) Stormandebo, and E) Lessebo.

6. Discussion

6.1. Visualization estimation for dNBR and dNDVI

The study aimed to investigate and re-evaluate the existing RS methodology for fire disturbance and forest health in a group of Fennoscandian boreal forests. To evaluate if the 2018 fire disturbance produced a strong enough signal to be captured, visualization methods were used and will be discussed in the following section. As stated in the methodology section, a proper analysis could not be conducted due to the small sample size. Thus, it is important to keep in mind that the results do not accurately represent the full potential of the methodology used in this study.

6.1.1. Did the 2018 boreonemoral forest wildfires produce a strong enough signal to be assessed using dNBR?

This study focused on using Sentinel-2 Copernicus product to estimate the burn severity using dNBR. Previous studies have revealed that this is a viable tool to assess the severity of forest wildfires for large-scale application (Keeley, 2009; Whitman, et al., 2018; Farasin, et al., 2020; UN, 2022). By analyzing the results, the burn severity is easily distinguishable for all sites, thus helping the user to identify the fire perimeter compared to the areal images (Appendix VII). The classification of burn severity shows the diversity of the fire damage within the fire border. Most fires showed moderate severity, concluding that some of the vegetation survived the 2018 fire disturbance. Only a few sites showed high-severity pixels within the burn scar, appreciating the total loss of vegetation within the 10 m by 10 m pixel (Figures 4 and 7). This is a robust estimation as there might be surviving trees within the pixel, but the overall value overlooks this factor.

Using dNBR values can help to minimize climate variability during the fire year as one of the precursors to fires is the drought effect revealing dry combustible biomass (Bickerton, 2012; Björklund, 2019; Wolters, 2022; WHO, 2022). This is minimized by taking pre-fire NBR values (2017) and subtracting post-fire NBR (2019) values. Even though this minimizes climate variability, it is vital to check that the pre-fire year and post-fire years are not categorized as drought years. Using dNBR in Swedish biomes proves to be a valuable tool to visualize the severity and total loss of biomass from the area.

6.1.2. Can an assessment be made for the boreonemoral forest health after the 2018 wildfire activity?

Looking at the dNDVI images for loss of vegetation between the pre-fire year and the end of the fire year shows a clear loss of vegetation within the entire image. This is supported by the fact that the drought year 2018 affected the entirety of Sweden, resulting in a loss of overall biomass. Looking within the fire perimeter, figures 9a, 10a, and 12a show no to little regrowth of vegetation within the border, except for the site

in Kil, where the control area shows loss of vegetation as well. The remaining sites show moderate regrowth concluding that there is a small reduction of vegetation production for the control plots. Unlike dNBR, the vegetation loss perimeter is larger for the sites Kil, Rullerum, and Stormandebo (Figures 9a, 10a, and 12a). But for the sites Lessebo and Österbymo, there is no indication of a fire perimeter at all (Figures 11a and 13a), concluding that the fire did not reach the canopy, and thus does not affect the NIR reflectance values for the sites.

The forest regeneration after the 2018 fire disturbance reveals most of the vegetation starts to recover to the 2017 pre-fire state. Even though there is a positive regrowth, it does not indicate the health of the trees, as it only measures the reflectance in the chlorophyll for green vegetation (Segah, et al., 2010; Lacouture, et al., 2020). Thus, the burn severity from the fire might have damaged the trees to a point where they cannot recover, allowing first succession dynamics to take hold again (Wallenius, et al., 2004; Sever, et al., 2012; Rolstad, et al., 2017). To better estimate tree health, the NDVI methodology needs to be modified and corrected for *Pinus sylvestris* tree reflectance to minimize this source of error.

6.2. Validation of RS methodology against ground measurements

To understand the correlation between burn severity and tree growth patterns it is vital to identify that the trees did take damage from the 2018 forest wildfires. Thus, the significance test between the burned and control plots allows the user to appreciate these changes. Previous studies have shown that forest wildfires create favorable conditions for the surviving trees but also other vegetation species (Wallenius, et al., 2004; Kasischke, et al., 2011; Rolstad, et al., 2017; Kuosmanen, et al., 2018). One way to identify if NDVI is a viable tool for this estimation is by identifying any correlation between growth patterns for the corresponding NDVI value. This would have been performed as stated in the data analysis but was not possible to do due to the small sample size. Thus, a visual correlation was made instead. This will be presented in the following section.

6.2.1. Can a correlation between high burn severity and low tree increment pattern be established?

To understand ARSTAN indices growth patterns, significance testing was done between burned and control plots for each year (Table 3). By looking at the statistical test, one can see a decrease in growth rate for both the burn and control plot between 2017 to 2018, corresponding to the drought effect happening in Sweden (Björklund, 2019; Granström, 2020). The mean value decreased for both plots indicating a disturbance happening. The 2019 burn plot shows a continuing decrease, thus hinting that the trees are healing from the fire disturbance. For the following years after 2019, the trees start to increase the increment pattern to a mean value of 0.0824, thus further confirming this theory (Wallenius, et al., 2004; Rolstad, et al., 2017).

The permutation test shows no statistical difference between the mean values of the burn and the control plot for the increment patterns for all years. This concludes that the mean values statistically are not different. Still, visually they are (Table 3). The year 2018 was considered one of the worst drought years Sweden faced in modern times, causing the trees in the control plots to be disturbed as well as in the burn plots. The results support that the extreme drought affected the entire area, as seen in the dNDVI for 2017-2018 (Figures 9a, 10a, 11a, 12a, and 13a) (Granström, 2020). Previous studies stated that a fire disturbance allows nutrients to be released back into the soil, and that creates favourable conditions for the surviving trees, which is confirmed in this study by looking at the mean values for 2021 (Wallenius, et al., 2004; Kasischke, et al., 2011; Rolstad, et al., 2017; Kuosmanen, et al., 2018).

Differences in dNBR between the burn and control plots showed statistical significance between them (Table 4). This can be seen for both the field sample burn values and the true middle burn values. Still, the effect size shows a bigger effect for the true middle burn values compared to the field sample burn values, concluding that there is a higher variance in dNBR values from the mean (Table 4). The lower dNBR values for the field sample burn plot might be due to the site selection for the burn plots, which too close to the fire borders causes pixels that are regarded as "outside the perimeter" to be included in the analysis.

As stated in the introduction to this section, an accurate correlation could not be established. Looking at Figure 8, one can see that the data points show no visual correlation between overall dNBR values to the corresponding growth increment. However, the control values show a cluster in the low dNBR values and a high growth increment value. This indicates that there might be a possible correlation if more samples are included. The site Lessebo shows interesting values, where a high growth rate and high dNBR values can be seen. This is of interest as this site includes the largest fire studied with the highest severity pixels overall. In Table 4, the difference in dNBR values can be seen, where the burn values show a high variance between the data. The true middle box shows values in the severity category (values ranging from ≈ 0.25 to ≈ 0.55, low to moderate severity). In contrast, the burn field sample value ranges from unburnt to moderate, indicating, as motioned before, that the field sample sites are too close to the fire border perimeter.

6.2.2. Can NDVI explain temporal changes to tree increment patterns for <u>Pinus sylvestris?</u>

Analyzing the statistical test for NDVI between the burned and control plots for all years showed no statistically significant difference except for the year 2019 (Table 5). The mean value between the control plots for all years showed a relatively low value (≈ 0.47), indicating moderate vegetation. Boreonemoral forest with dominating *Pinus sylvestris* trees tends to grow on dry soils with a continental climate, where this type of forest can be found on dry, rocky alluvial heaths (Esseen, et al., 1997) (Appendix VIII). Looking at the mean value for the burned plot between all the years, one can see a

higher NDVI value (≈ 0.53) in 2017 compared to the control plot. Looking at the images from the field sampling, it is evident that the burned and control plots vary, which might explain the differences in the NDVI values (Appendix VIII).

The NDVI values for the burn plots for all years show a decline from 2018 to 2020, indicating an overall loss of abundant vegetation in the area. The difference between the pre-fire state (2017) and the 2020 value shows roughly a decrease of 0.203, compared to the reduction of only 0.056 for the control plot. This supports that the fire had a more significant effect on the burned plot than the drought effect for NDVI, which was hypothesised for the dNBR values. Thus, NDVI is a valuable indicator to estimate the impact and regrowth of trees after disturbance than dNBR alone. For the year 2019, the difference between burned and control plots could be established using the permutation test, where the p-value was 0.04, which indicates that in 2019 the disturbance could be detected by the NDVI values.

By looking if there is a visual correlation between NDVI and the growth increments in Figure 14, we can conclude that no relationship could be established. Similar trend patterns (only for 1-2 years) can be seen between the different variables for all sites but are not strong enough to establish a correlation. For the sites, Kil, Österbymo, and Stormandebo (Figures 14a, 14c, and 14d, respectively) show an apparent decline in growth increment between 2017 and 2018 for the control and burn plot. For Stormandebo, this trend is also seen for NDVI control and burned values before they divert from each other again. Lessebo shows a diversion between control and burned plot increment growth. The control decreased between 2017 and 2018, while the burn decreased between 2019 and onward (Figure 14e). This might indicate that the trees affected by the fire started to show damage much later and could not recover from the injury creating secondary mortality (Heikkala, et al., 2014). Looking at Rullerum (Figure 14b), the burn plots' increment growth peaked between 2017 and 2018, like Lessebo (Figure 14e), where the NDVI values for the burned also followed this same pattern. Even though this study cannot conclude if a correlation can be established, similarities have been identified (Kaufmann, et al., 2008; Bhuyan, et al., 2017).

6.2.3. Future development

As this is a pilot project, the analysis of dNBR, dNDVI, and NDVI, with their corresponding tree increment values, could not correctly be executed due to the small sample size (see Chapter. 4.4. *Data analysis*). For future studies, it is vital to have a larger sample size of field samples and their related satellite imagery. For field samples, it is purposed to core a minimum of 20 trees (10 for burned plot and 10 from a control site) with two cores for each tree (to ensure that the rings are correctly measured). The table seen below (Table 6) shows a rough estimate of how much time it would take to process 40 cores and their related satellite imagery (one site). This paper considered five sites located in the southeast of Sweden, but it is recommended to use a minimum of 10 sites to ensure an accurate assessment.

The table does not consider the travel time to and from sites, as all sites are located differently depending on where you are situated. The timetable assessment does not include prior knowledge of the programs used and code development.

Table 6: Timetable showing the total time it takes to collect, process, and analyse one field site. One site includes 40 cores (from burned and corresponding control plots) and related satellite imagery. This table does not include travel time.

	Time table			
Activity	**Preperation**	**Collecting**	**Processing**	**Analysis**
	RS processing			
Sentinel-2 Coperenicus data	1	2	3	4
	Field work			
Tree increments	1	12	10	6
Total time (Hours):	**39**			

6.3. Can we use RS methodology for assessing burn severity and forest regrowth?

The usage of RS methodology is a potential tool for burn severity assessment and forest regrowth estimation for boreal forests in Fennoscandia (White, et al., 1996; Isaev, et al., 2002; Kaufmann, et al., 2008; Li, et al., 2010; Sherstjuk, et al., 2018; Bhuyan, et al., 2017; McKenna, et al., 2018; Whitman, et al., 2018; UN, 2022). RS tools have been proven to work in other boreal forests across the globe, but as with all methods, they must be adapted to the study area. Climate variability can pose a problem as space-borne imagery is sensitive to atmospheric noise from the present atmosphere (Beck, et al., 2007). Spatial resolution is also an essential factor for evaluating the tool, as the low spatial resolution does not capture the variability within the pixels. Temporal resolution poses a problem as the return time might be captured at different times and with too big-time gaps. Sentinel-2 Copernicus's mission fulfils the demand for both spatial and temporal resolution combined (ESA, u.d.). The future NBR and NDVI methodology needs to be corrected for the boreal forests in Sweden with more data to determine if there is a correlation between tree growth patterns and the proposed methods presented.

Finally, the site variability must be considered. All sites vary in soil structure, moisture availability, and nutrient availability (Angelstam, 1998; Bickerton, 2012; Wolters, 2022; WHO, 2022). Multiple factors contribute to why some forests are prone to fires, and others are not (Angelstam, 1998). Understanding these factors will help us assess the effect of fires on tree growth in Sweden and improve the global C budget for the future climate.

7. Summary and conclusion

The study investigated and evaluated existing RS methodology for fire disturbance in a group of Swedish boreonemoral forests. Estimating burn severity (dNBR) on boreonemoral forests show good potential as the fire disturbance signal is captured using Sentinel-2 images. The fire signal is clear for all fires where the smaller ones were also captured in this study. Fires with moderate to high severity show better performance when using dNBR. dNDVI, like dNBR, showed a clear signal where the fire disturbances were captured and other disturbances like the 2018 drought effect. dNDVI showed promising results as the fire location is clearly visible, but the fire borders differ from the dNBR maps. Analysis of the 2018 forest wildfires' impact by looking at dNDVI images showed that the vegetation returned to a near pre-fire state (2017). But dNDVI measures the entirety of the forest vegetation. Thus, this needs to be modified to reflect the health accurately for the Pine trees. Using the presented RS methodology for visualisation (dNBR and dNDVI) is viable as it helps users visualise the effects and severity of boreal forest wildfires and vegetation recovery.

Using dNBR as a tool to estimate burn severity patterns has been proven possible but unreliable regarding the relationship between high burn severity and decreased tree increment patterns. As this study concluded that more samples are needed to establish if there is a relationship between dNBR and tree increment patterns. NDVI temporal changes have been shown to explain some of the changes to Pine increment patterns but are restricted to 1–2-year trends. The fire year 2018 affected the increment patterns for all study sites. Still, the effect was also present in the following years, 2019 and 2020, indicating that secondary disturbances are affecting the individual sites. However, NDVI might be reliable for evaluating temporal growth increment patterns in Swedish boreonemoral forests. Due to the few sites, this cannot be confirmed or denied.

Both presented RS methods are robust but need modifying as variabilities in reflectance can be uncertain. The usage of RS methodology shows potential for the future, as improvements can be made from this pilot study to validate the presented method better. An increase in global mean air temperature will affect the frequency of wildfire regimes. It is predicted that the increase in wildfire regimes will impact the global C budget, as stored C in soils and biomass will be released back into the atmosphere more rapidly. The presented RS methodology is a valuable and powerful tool for a better understanding this relationship and further improvement of the global C budget.

References

Akther, S. M., & Hassan, Q. K. (2011, 10 10). Remote Sensing-Based Assessment of Fire Danger Conditions Over Boreal Forest. *IEEE Journal of selected Topics in Applied Earth Observations and Remote Sensing, 4*(4), 992-999.

Alexander, M. E., & Cruz, M. G. (2019). Fireline Intensity. In S. L. Manzello, *Encyclopedia of Wildfires and Wildland-Urban Interface (WUI) Fires.* Springer.

Alkhatib, A. A. (2014, 03 04). A Review on Forest Fire Detection Techniques. *International Journal of Distributed Sensor Networks, 10*(3).

Angelstam, P. K. (1998). Maintaining and restoring biodiversity in European boreal forests by developing natural disturbance regimes. *Journal of Vegetation Science, 9*, 593-602.

Bäckström, L., & Grenert, P. (2019). *Damage Assessment of the 2018 Swedish Forest Fires Using Sentinel-2 and Pleiades Data.* Teknik, Vetenskap och Konst. Stockholm: KTH .

Beck, P. S., Jönsson, P., Høgda, K. -A., Karlsen, S. R., Eklundh, L., & Skidmore, A. K. (2007). A ground-validated NDVI dataset for monitoring vegetation dynamics and mapping phenology in Fennoscandia and the Kola peninsula. *International Journal of Remote Sensing, 28*(19).

Bhuyan, U., Zang, C., Vicente-Serrano, S. M., & Menzel, A. (2017, 05 25). Exploring Relationships among Tree-Ring Growth, Climate Variability, and Seasonal Leaf Activity on Varying Timescales and Spatial Resolutions. *Remote sensing, 9*, 526-539.

Bickerton, J. (2012). The fire triangle. *Loss Prevention Bulletin*(226), 6-11.

Björheden, R., & Johannesson, T. (2019). *Effekter på svenskt skogsbruk av sommaren 2018.* Uppsala Science Park. Uppsala: Skogforsk.

Bräker, O. U. (2002). Measuring and data processing in tree-ring research – a methodological introduction. *Dendrochronologia, 20*(1-2), 203-216.

Chiu, B., Roy, R., & Tran, T. (2022). Wildfire Resiliency: California Case for Change. *IEEE Power and Energy Magazine, 20*(1), 28-37.

Chuvieco, E., Cocero, D., Riano, D., Martin, P., Martinez-Vega, J., de la Riva, J., & Pérez, F. (2004, 08 30). Combining NDVI and surface temperature for the estimation of live fuel moisture content in forest fire danger rating. *Remote sensing of Enviroment, 92*(3), 322-331.

Cook, E. R., & Holmes, R. L. (1999). *Program ARSTAN*. Retrieved 05 2022, from https://www.ltrr.arizona.edu/~sheppard/DISC2019/arstan.txt

De Simone, W., Di Musciano, M., Di Cecco, V., Ferella, G., & Frattaroli, A. R. (2020, 04 13). The potentiality of Sentinel-2 to assess the effect of fire events on Mediterranean mountain vegetation. *Plant Sociology, 57*(1), 11-22.

Eckdahl, J., Kristensen, A. J., Metcalfe, B. D. (2022, 05 13). Climatic variation drives loss and restructuring of carbon and nitrogen in boreal forest wildfire. *Biogeosciences, 19* (9), 2487-2506.

Edvardsson, J., Baužiene, I., Lamentowicz, M., Šimanauskienė, R., Tamkevičiūtė, M., Taminskas, J., . . . Stoffel, M. (2019). A multi-proxy reconstruction of moisture dynamics in a peatland ecosystem: A case study from Čepkeliai, Lithuania. *Ecological Indicators, 106.*

Eriksson, A., Frisk, A., Hansson, L., & Nilsson, L. (2018). *Förslag till åtgärder för att kompensera drabbade i skogsbruket för skador med anledning av skogsbränderna sommaren 2018.* Skogsstyrelsen.

ESA. (2022, 03 05). *Overview*. Retrieved from Sentinel Online: https://sentinel.esa.int/web/sentinel/missions/sentinel-2/overview

ESA. (n.d.). *Sentinel-2*. Retrieved 04 2022, from esa: https://sentinel.esa.int/web/sentinel/missions/sentinel-2

Esseen, P.-A., Ehnström, B., Ericson, L., & Sjöberg, K. (1992). Climate and Hydrology of Some Fennoscandian Tundra Ecosystems. In L. (eds) Hansson, *Ecological Principles of Nature Conservation* (pp. 252-325). Boston, MA: Springer.

Esseen, P.-A., Ehnström, B., Ericson, L., & Sjöberg, K. (1997). Boreal forests. *Ecological Bulletins, 46*, 16-47.

Farasin, A., Colomba, L., & Garza, P. (2020). Double-Step U-Net: A Deep Learning-Based Approach for the Estimation of Wildfire Damage Severity through Sentinel-2 Satellite Data. *Applied Science (Intelligence Systems and Sensors), 10*(12).

GEE. (2022, 02 18). *Google Earth Engine*. Retrieved from Google Earth Engine: https://earthengine.google.com

GEE. (2022, 02 23). *A planetary-scale platform for Earth science data & analysis*. Retrieved from Earth Engine Data Catalog: https://developers.google.com/earth-engine/datasets/

GISGeography. (2021, 10 29). *What is NDVI (Normalized Difference Vegetation Index)?* Retrieved from GISGeography: https://gisgeography.com/ndvi-normalized-difference-vegetation-index/

Global Forest Watch. (2022, 01 30). *Fires*. Retrieved from Global Forest Watch: https://www.globalforestwatch.org/topics/fires/#intro

Google Earth. (2022, 03 03). *Google Earth*. Retrieved from Google Earth: https://www.google.com/intl/sv/earth/versions/

Granström, A. (2020). *Brandsommaren 2018 – Vad hände, och varför?* SLU. Myndigheten för samhällsskydd och beredskap (MSB).

Haglöf Sweden . (2022, 04 21). *Increment borers*. Retrieved from Haglöf Sweden: https://haglofsweden.com/project/increment-borers/

Heikkala, O., Suominen, M., Junninen, K., Hämäläinen, A., Kouki, J. (2014). Effects of retention level and fire on retention tree dynamics in boreal forests. *Forest Ecology and Management*, *328,* 193-201.

Høgda, K. A., Tømmervik, H., & Karlsen, S. R. (2013). Trends in the Start of the Growing Season in Fennoscandia 1982–2011. *Remote Sensing, 5*(9), 4304-4318.

Holden, S. R., Rogers, B. M., Treseder, K., & Randerson, J. T. (2016, 02 23). LETTER • THE FOLLOWING ARTICLE IS OPEN ACCESS Fire severity influences the response of soil microbes to a boreal forest fire. *Enviromental Research Letters, 11*(3).

IPCC. (2019). *Summary for Policymakers. In: Climate Change and Land: an IPCC special report on climate change, desertification, land degradation, sustainable land management, food security, and greenhouse gas fluxes in terrestrial ecosystems [P.R. Shukla, J. Skea, E.* IPCC.

IPCC. (2021). *Summary for Policymakers. In: Climate Change 2021: The Physical Science Basis. Contribution of Working Group I to the Sixth Assessment Report of the Intergovernmental Panel on Climate Change [MassonDelmotte, V., P. Zhai, A. Pirani, S.L. Connors, C. Péan,.* Cambridge University Press.

Isaev, A., Korovin, G., Bartalev, S., Ershov, D., Janetos, A., Kasischke, E., . . . Murphy, T. (2002). USING REMOTE SENSING TO ASSESS RUSSIAN FOREST FIRE CARBON EMISSIONS. *Climate change, 55*, 235-249.

Jones, M. W., Smith, A., Betts, R., Canadell, J. G., Prentice, C. I., & Quéré, L. (2020, 01 14). *Climate Change Increases the Risk of Wildfires.* Retrieved 11 2021, from ScienceBrief Review: https://sciencebrief.org/briefs/wildfires

Karlsen, S. R., Høgda, K. A., Wielgolaski, F. E., Tolvanen, A., Tømmervik, H., Poikolainen, J., & Kubin, E. (2009, 09). Growing-season trends in Fennoscandia 1982–2006, determined from satellite and phenology data. *Climate Research, 39*(3), 275-286.

Kasischke, E. S., Bergen, K., Fennimore, R., Sotelo, F., Stephens, G., Janetos, A., & Shugart, H. H. (2011). Satellite imagery gives clear picture of Russia's boreal forest fires. *Eos, Transactions American Geophysical Union, 80*(13), 141-147.

Kaufmann, R. K., D'Arrigo, R. D., Paletta, L. F., Tian, H., Jolly, W. M., & Myneni, R. B. (2008, 10). Identifying Climatic Controls on Ring Width: The Timing of Correlations between Tree Rings and NDVI. *Earth Interactions, 12*(14), 1-14.

Keeley, J. E. (2009, 01). Fire intensity, fire severity and burn severity: A brief review and suggested usage. *International Journal of Wildland Fire, 18*(1), 116-126.

Kelhä, V., Rauste, Y., Häme, T., Sephton, T., Buongiorno, A., Frauenberger, O., . . . Vainio, T. (2003). Combining AVHRR and ATSR satellite sensor data for operational boreal forest fire detection. *International Journal of Remote Sensing, 24*(8), 1691-1708.

Krisinformationen. (2018, 08 27). *Skogsbränderna 2018*. Retrieved from Krisinformationen: https://www.krisinformation.se/detta-kan-handa/handelser-och-storningar/2018/brandrisk2018

Krol, L. R. (2021, 01 13). *Permutation Test*. Retrieved 06 2022, from MathWorks: https://www.mathworks.com/matlabcentral/fileexchange/63276-permutation-test

Kuosmanen, N., Marquer, L., Tallavaara, M., Molinari, C., Zhang, Y., Alenius, T., Seppä, H. (2018, 02 17). The role of climate, forest fires and human population size in Holocene vegetation dynamics in Fennoscandia. *Journal of Vegetation Science, 29*(3), 382-392.

Lacouture, D. L., Broadbent, E. N., & Crandall, R. M. (2020, 05 20). Detecting Vegetation Recovery after Fire in A Fire-Frequented Habitat Using Normalized Difference Vegetation Index (NDVI). *Forests (Remote Sensing of Forest Disturbances and Recovery), 11*(7).

Lange, M., Dechant, B., Rebmann, C., Vohland, M., Cuntz, M., & Doktor, D. (2017, 08 11). Validating MODIS and Sentinel-2 NDVI Products at a Temperate Deciduous Forest Site Using Two Independent Ground-Based Sensors. *Sensors, 17*(8), 1855-.

Leica. (2022, 05). *Stereo Microscopes & Macroscopes*. Retrieved from Leica: https://www.leica-microsystems.com/products/stereo-microscopes-macroscopes/

Li, Z., Nadon, S., & Cihlar, J. (2010). Satellite-based detection of Canadian boreal forest fires: Development and application of the algorithm. *International Journal of Remote Sensing, 21*(16), 3057-3069.

Llorens, R., Sobrino, J. A., Fernández, C., Fernández-Alonso, J. M., & Vega, J. A. (2021). A methodology to estimate forest fires burned areas and burn severity degrees using Sentinel-2 data. Application to the October 2017 fires in the Iberian Peninsula. *International Journal of Applied Earth Observation and Geoinformation, 95*.

Martell, D. L. (2007). Forest Fire Management. In A. Weintraub, C. Romero, T. Bjorndal, & R. Epstein, *Handbook of Operations Research in Natural Resources* (Vol. 99, pp. 489-509). Boston, MA: Springer.

MatLab. (n.d.). *MatLab*. Retrieved 03 12, 2021, from MatLab: https://uk.mathworks.com/products/matlab.html

McKenna, P., Phinn, S., & Erskine, P. D. (2018). Fire Severity and Vegetation Recovery on Mine SiteRehabilitation Using WorldView-3 Imagery. *Fire, 1*(2).

Milz, M. (2013). *STUDY ON FOREST FIRE DETECTION WITH SATELLITE DATA.* Rymdteknik Institutionen f¨or System- och rymdteknik (SRT). Kiruna: Luleå Tekniska Universitet.

Moen, A., & Lillethun, A. (1999). *National atlas of Norway : vegetation.* Hønefoss: Norwegian Mapping Authority.moisture dynamics in a peatland ecosystem: A case study from Čepkeliai, Lithuania. *Ecological Indicators, 106*.

Molinari, C., Carcaillet, C., Bradshaw, R. H., Hannon, G. E., & Lehsten, V. (2020, 08 01). Fire-vegetation interactions during the last 11,000 years in boreal and cold temperate forests of Fennoscandia. *Quaternary Science Reviews, 241*.

Økland, R. H. (1990). *Sommerfeltia Supplement 1.* Oslo: University of Oslo.

Quintano, C., Fernández-Manso, A., & Fernández-Manso, O. (2018, 02). Combination of Landsat and Sentinel-2 MSI data for initial assessing of burn severity. *International Journal of Applied Earth Observation and Geoinformation, 64*, 221-225.

Rinn, F. (2003). *TSAP-Win™ Time series analysis software*. Retrieved 05 2022, from Rinntech: https://rinntech.info/products/tsap-win/

Rinn, F. (n.d.). *LinTab™ Modular tree ring measuring stages*. Retrieved 05 2022, from Rinntech: https://rinntech.info/products/lintab/

Rolstad, J., Blanck, Y.-l., & Storaunet, K. O. (2017, 02 21). Fire history in a western Fennoscandian boreal forest as influenced by human land use and climate. *Ecological Monographs, 87*(2), 219-245.

Segah, H., Tani, H., & Hirano, T. (2010, 10 20). Detection of fire impact and vegetation recovery over tropical peat swamp forest by satellite data and ground-based NDVI instrument. *International Journal of Remote Sensing, 31*(20), 5297-5314.

Sever, L., Leach, J., & Bren, L. (2012, 12 03). Remote sensing of post-fire vegetation recovery; a study using Landsat 5 TM imagery and NDVI in North-East Victoria. *Journal of Spatial Science, 57*(2), 175-191.

Sherstjuk, V., Zharikova, M., & Sokol, I. (2018). Forest Fire-Fighting Monitoring System Based on UAV Team and Remote Sensing. *IEEE 38th International Conference on Electronics and Nanotechnology (ELNANO)*, 663-668.

Shi, G., Yan, H., Zhang, W., Dodson, J., Heijnis, H., & Burrows, M. (2021). Rapid warming has resulted in more wildfires in northeastern Australia. *Science of The Total Enviroment, 771*.

Skartveit, A., Rydén, B. E., & Kärenlampi, L. (1975). Climate and Hydrology of Some Fennoscandian Tundra Ecosystems. *Fennoscandian Tundra Ecosystems*, 41-53.

Skogsstyrelsen. (2022, 02 25). *Kartor*. Retrieved from Kartor: https://kartor.skogsstyrelsen.se/kartorapp/?startapp=brandkartan

SMHI. (2019, 04 18). *Året 2018 - Varmt, soligt och torrt år*. Retrieved from SMHI: https://www.smhi.se/klimat/2.1199/aret-2018-varmt-soligt-och-torrt-ar-1.142756

Statens Offentliga Utredningar. (2019). *Skogsbränderna sommaren 2018.* Stockholm: Elanders Sverige AB.

Sunar, F., & Özkan, C. (2001). Forest fire analysis with remote sensing data. *International Journal of Remote Sensing, 22*(12), 2265-2277.

UCDavis. (2022, 05 04). *Wildfire*. Retrieved from UCDavis: https://climatechange.ucdavis.edu/climate/definitions/wildfire

UN. (2022, 02 01). *Forest Fire*. Retrieved from United Nations : https://www.un-spider.org/disaster-type/forest-fire

UN. (2022, 02 06). *Normalized Burn Ratio (NBR)*. Retrieved from United Nations: https://un-spider.org/advisory-support/recommended-practices/recommended-practice-burn-severity/in-detail/normalized-burn-ratio

USGS. (2022, 02 28). *How much distance does a degree, minute, and second cover on your maps?* Retrieved from USGS: https://www.usgs.gov/faqs/how-much-distance-does-degree-minute-and-second-cover-your-maps#:~:text=One%20degree%20of%20latitude%20equals,one%20second%20equals%2080%20feet.

Wallenius, T. H., Kuuluvainen, T., & Vanha-Majamaa, I. (2004, 07). Fire history in relation to site type and vegetation in Vienansalo wilderness in eastern Fennoscandia, Russia. *Canadian Journal of Forest Research, 34*, 1400-1409.

White, J. D., Ryan, K. C., Key, C. C., & Running, S. W. (1996). Remote Sensing of Forest Fire Severity and Vegetation Recovery. *Wildland Fire, 6*(3), 125-136.

Whitman, E., Parisien, M.-A., Thompson, D. K., Hall, R. J., Skakun, R. S., & Flannigan, M. D. (2018). Variability and drivers of burn severity in the northwestern Canadian boreal forest. *Ecosphere, 9*(2).

WHO. (2021, 11 26). *Wildfires*. Retrieved from World Health Organization: https://www.who.int/health-topics/wildfires#tab=tab_1

Wolters, C. (2022, 03 29). *Here's how wildfires get started—and how to stop them*. Retrieved from National Geographic: https://www.nationalgeographic.com/environment/article/wildfires

Appendix

Appendix I: Code for converting point coordinates to rectangles.

Code for converting point coordinates to rectangles using MATLAB.

```
%% Script to convert point coordinates to rectangle.

% Written by Joanna Eaton & Veiko Lehsten 2022.

%% Conversion of point to rectangle.

% Distance of intrest.

meter = 3000;

% Point coordinates for one site.

PointLo = Longitude; % Longitude point.
PointLa = Latitude; % Latitude point.

% Conversion.

old_dist=0;

for dy=0.0001:0.00001:0.02
    north_south=lldistkm([PointLo PointLa-dy ],[PointLo PointLa+dy ])  ;
    if old_dist<meter/1000 & north_south>meter/1000
        GeoCoorLat=dy;
        break
    else
        old_dist=north_south;
    end
end

old_dist=0;

for dx=0.0001:0.000001:0.02
    east_west=lldistkm([PointLo-dx PointLa ],[PointLo+dx PointLa ])
    if old_dist<meter/1000 & east_west>meter/1000
        GeoCoorLong=dx;
        break
    else
        old_dist=east_west;
    end
end

GeoLo1 = PointLo + GeoCoorLong;
GeoLo2 = PointLo - GeoCoorLong;

GeoLa1 = PointLa + GeoCoorLat;
GeoLa2 = PointLa - GeoCoorLat;

Coordinat_86 = [GeoLo1 GeoLo2 GeoLa1 GeoLa2]; % Data stored in this matrix.

north_south_86=lldistkm([GeoLo1 GeoLa1 ],[GeoLo1 GeoLa2])
east_west_86=lldistkm([GeoLo1 GeoLa1 ],[GeoLo2 GeoLa1])
```

Appendix II: GEE code for downloading the images.

GEE code for downloading images from Sentinel-2 using Java Script. The code includes filters such as start and end date, cloud filter, and scale.

```
// Code for downloading Satellite Imaging from GEE.
// The code is produced by Joanna Eaton and Veiko Lehsten 2022.


// This section specifies area of intrest and available data for that region.
var geometryfire  = ee.Geometry.Rectangle([ 16.310544000000000,   57.756471000000000,  16.292555999999998,  57.737731000000004]); // Area of intrest.
var batch = require('users/fitoprincipe/geetools:batch') // Geotool for batch collection.

var collection2S = ee.ImageCollection("COPERNICUS/S2") // Satellite images based on area of intrest, timeframe, and cloud percentage.
  .filterBounds(geometryfire)
   .filterDate('2017-05-01', '2017-09-01')
    .filter(ee.Filter.lte('CLOUDY_PIXEL_PERCENTAGE',100));
print(collection2S);


// Export the image, specifying scale and region.

batch.Download.ImageCollection.toDrive(collection2S,
  "Site86_17",
  {description: 'Fire_2017S2',
  region: geometryfire,
  fileFormat: 'GeoTIFF',
  scale : 10,
  formatOptions: {
    cloudOptimized: true
  }

});
```

Appendix III: Table showing the complete list of tree cores.

Table over all tree increment cores used in the project. The table also includes tree ID, their core ID, location (longitude and latitude), burn scar height, as well as crown mortality. The table is divided between burn and control sites.

Burn						Unburnt			
Tree_ID	Core_ID	Longitude	Latitude	Burn_Scar	Crown_Mortality(%)	Tree_ID	Core_ID:	Longitude	Latitude
71_1_1	948091	13.247778	59.597365	2.3	NaN	72_1_1	948141	13.249393	59.596579
71_1_2	948092	13.247778	59.597365	2.3	NaN	72_1_2	948142	13.249393	59.596579
71_2_1	948101	13.247884	59.597463	2.5	NaN	72_2_1	948151	13.249380	59.596544
71_2_2	948102	13.247884	59.597463	2.5	NaN	72_2_2	948152	13.249380	59.596544
71_3_1	948111	13.247959	59.597667	2.9	NaN	72_3_1	948161	13.249672	59.596649
71_3_2	948112	13.247959	59.597667	2.9	NaN	72_3_2	948162	13.249672	59.596649
71_4_1	948121	13.248006	59.597457	1.95	NaN	72_4_1	948171	13.249470	59.596661
71_4_2	948122	13.248006	59.597457	1.95	NaN	72_4_2	948172	13.249470	59.596661
71_5_1	948131	13.247817	59.597087	3.5	NaN	72_5_1	948181	13.249342	59.596711
71_5_2	948132	13.247817	59.597087	3.5	NaN	72_5_2	948182	13.249342	59.596711
83_1_1	948351	15.350733	57.808759	1.10	NaN	84_1_1	948301	15.350466	57.807965
83_1_2	948352	15.350733	57.808759	0.3	NaN	84_1_2	948302	15.350466	57.807965
83_2_1	948361	15.350963	57.808920	0.4	100	84_2_1	948311	15.350233	57.808006
83_2_2	948362	15.350963	57.808920	0.4	100	84_2_2	948312	15.350233	57.808006
83_3_1	948371	15.351020	57.808952	0.5	NaN	84_3_1	948321	15.350278	57.808048
83_3_2	948372	15.351020	57.808952	0.5	NaN	84_3_2	948322	15.350278	57.808048
83_4_1	948381	15.350805	57.809039	0.4	NaN	84_4_1	948331	15.350190	57.808041
83_4_2	948382	15.350805	57.809039	0.4	NaN	84_4_2	948332	15.350190	57.808041
83_5_1	948391	15.350738	57.809112	0.15	NaN	84_5_1	948341	15.350246	57.808278
83_5_2	948392	15.350738	57.809112	0.15	NaN	84_5_2	948342	15.350246	57.808278
81_1_1	948201	16.617150	58.267692	1.5	100	82_1_1	948251	16.617464	58.266943
81_1_2	948202	16.617150	58.267692	1.5	100	82_1_2	948252	16.617464	58.266943
81_2_1	948211	16.617386	58.267737	2.5	30	82_2_1	948261	16.617475	58.266859
81_2_2	948212	16.617386	58.267737	2.5	30	82_2_2	948262	16.617475	58.266859
81_3_1	948221	16.617657	58.267702	1.95	NaN	82_3_1	948271	16.617631	58.266797
81_3_2	948222	16.617657	58.267702	1.95	NaN	82_3_2	948272	16.617631	58.266797
81_4_1	948231	16.617303	58.267706	2.8	20	82_4_1	948281	16.617313	58.266757
81_4_2	948232	16.617303	58.267706	2.8	20	82_4_2	948282	16.617313	58.266757
81_5_1	948241	16.617496	58.266734	2	NaN	82_5_1	948291	NaN	NaN
81_5_2	948242	16.617496	58.266734	2	NaN	82_5_2	948292	NaN	NaN
85_1_1	948401	16.301705	57.746654	1.5	60	86_1_1	948451	16301423	57.747037
85_1_2	948402	16.301705	57.746654	1.5	60	86_1_2	948452	16301423	57.747037
85_2_1	948411	16.301576	57.746737	1.8	NaN	86_2_1	948461	16.301650	57.747137
85_2_2	948412	16.301576	57.746737	1.8	NaN	86_2_2	948462	16.301650	57.747137
85_3_1	948421	16.301379	57.746635	5.5	NaN	86_3_1	948471	16.301849	57.747115
85_3_2	948422	16.301379	57.746635	5.5	NaN	86_3_2	948472	16.301849	57.747115
85_4_1	948431	16.301694	57.746635	1	NaN	86_4_1	948481	16.301555	57.747052
85_4_2	948432	16.301694	57.746635	1	NaN	86_4_2	948482	16.301555	57.747052
85_5_1	948441	16.301889	57.746913	1.8	NaN	86_5_1	948491	16.301638	57.747035
85_5_2	948442	16.301889	57.746913	1.8	NaN	86_5_2	948492	16.301638	57.747035
99_1_1	948001	15.431093	56.871761	NaN	100	100_1_1	948041	15.428578	56.871996
99_1_2	948002	15.431093	56.871761	NaN	100	100_1_2	948042	15.428578	56.871996
99_2_1	948011	15.431062	56.871771	NaN	100	100_2_1	948051	15.428694	56.872058
99_2_2	948012	15.431062	56.871771	NaN	100	100_2_2	948052	15.428694	56.872058
99_3_1	948021	15.431109	56.871809	2.5	66.66	100_3_1	948061	15.428758	56.871992
99_3_2	948022	15.431109	56.871809	2.5	66.66	100_3_2	948062	15.428758	56.871992
99_4_1	948031	15.431154	56.871745	5.4	33.33	100_4_1	948071	15.428709	56.871921
99_4_2	948032	15.431154	56.871745	5.4	33.33	100_4_2	948072	15.428709	56.871921
						100_5_1	948081	15.428647	56.871936
						100_5_2	948082	15.428647	56.871936

Appendix IV: Code for keeping or discarding satellite imagery

Code for keeping or discarding satellite images in red greed blue composition. This allows the user to discard images of low quality. This code was produced by Veiko Lehsten. The code is written in MATLAB.

```
%% Code for viewing images and discarding images of low quality

% Code is written by Veiko Lehsten 2022.
% Press 1 to keep the image, press 2 if the images are of low quality, and press 0 to delete
% the image from the folder.

%% Keep or Discard

close all
folder_name=''; % Keep empty.


dirimages=dir(['500x500_2021/Site21_100' folder_name ]) % Add in folder path and to all the other places with the same ID.
last_day='123';

% Code loops through the entire folder for images.

for i=3:size(dirimages,1)
    if ~dirimages(i).isdir
        if ~strcmp(dirimages(i).name(1:8),last_day)
            im=imread(['500x500_2021/Site21_100'  folder_name '/', dirimages(i).name]);
            last_day=dirimages(i).name(1:8);

            % To view the images in RGB.
            A = im;
            RGBImage  = A(:,:,[4 3 2]);
            RGBImage = uint8(rescale(RGBImage, 0, 255));
            imshow(RGBImage);
            set(gcf, 'PaperPosition', [0 0 4 2]);

            % Use if you want to view the images in a specific band.

            %imgesc(squeeze(im(:,:,8));

            x=input('keep ? 0: no 1:yes good quality  2: bad quality');
            if x==2         % Low quality images
                evalc(['! mv 500x500_2021/Site21_100'  folder_name '/', dirimages(i).name ' 500x500_2021/Site21_100'  folder_name '/low_quality/' ]);
            end
            if ~x
                delete(['500x500_2021/Site21_100'  folder_name '/', dirimages(i).name]);

            end

             if x==1          % Keep the image
                 datum_name = [dirimages(i).name(1:4)  '-' dirimages(i).name(5:6) '_' dirimages(i).name(7:8) ];
                 eval(['! cp  500x500_2021/Site21_100'  folder_name '/', dirimages(i).name ' 500x500_2021/Site21_100'  folder_name '/high_quality/' datum_name '.tif'  ])
             end
        else
             delete(['500x500_2021/Site21_100'  folder_name '/', dirimages(i).name]);
        end
        end
end
```

Appendix V: Processing code for RS methodology

MATLAB script for the entire RS processing for the thesis. The code includes converting .tif to MATLAB matrix, dNBR, dNDVI, and NDVI. The code also includes how the images was produced, analysis of the RS method, and tree increment alaysis.

```
%% Script to import, calculate, and display figures

% Script developed by Joanna Eaton 2022.
% Credits to Wenxin Zhang & Veiko Lehsten.

%% Import and process satellite images.

% This code loops through the folders and reads the data in them (each
% Sentinel-2 images.

% The data is also stored as NDVI & NBR files in 3D-matrixes with all the NDVI & NBR values for
% all sites. NDVI is averaged over the site.

% Site 72 (Kil).
display('Site 72');

for i=72  % Folder tick

if (i<=72||i>=74)
Path=['/Users/joeaton/Desktop/MatLab modelling/Masterthesis/500x500_17/Site17_',num2str(i)];   % Folder path to where the data is stored
File=dir(fullfile(Path,'*.tif'));              % Open the .tif ending files
FileNames={File.name}';                        % Rename and locates it in a filename string matrix
leng=size(FileNames,1);                        % Loops through the length of the File matrix
for j= 1:leng
[GISImg_72,Ref72] = geotiffread([Path,'/', cell2mat(FileNames(j))]);                          % Loops through MatLab GEOTiff format
NDVI_temp=(GISImg_72(:,:,8)-GISImg_72(:,:,4))./(GISImg_72(:,:,8)+GISImg_72(:,:,4));     % Calculating the NDVI values
NDVI84_18(:,:,j)=NDVI_temp;                                                              % Stores the NDVI values in 3D

NBR_temp=(GISImg_72(:,:,8)-GISImg_72(:,:,12))./(GISImg_72(:,:,8)+GISImg_72(:,:,12));
NBR84_18(:,:,j)=NBR_temp;


end

end
end

% Site 82 (Stormandebo)
display('Site 82');

for i=82  % Folder tick

if (i<=72||i>=74)
Path=['/Users/joeaton/Desktop/MatLab modelling/Masterthesis/500x500_17/Site17_',num2str(i)];   % Folder path to where the data is stored
File=dir(fullfile(Path,'*.tif'));              % Open the .tif ending files
FileNames={File.name}';                        % Rename and locates it in a filename string matrix
leng=size(FileNames,1);                        % Loops through the length of the File matrix
for j= 1:leng
[GISImg_82,Ref82] = geotiffread([Path,'/', cell2mat(FileNames(j))]);                          % Loops through MatLab GEOTiff format
NDVI_temp=(GISImg_82(:,:,8)-GISImg_82(:,:,4))./(GISImg_82(:,:,8)+GISImg_82(:,:,4));     % Calculating the NDVI values
NDVI84_18(:,:,j)=NDVI_temp;                                                              % Stores the NDVI values in 3D

NBR_temp=(GISImg_82(:,:,8)-GISImg_82(:,:,12))./(GISImg_82(:,:,8)+GISImg_82(:,:,12));
NBR84_18(:,:,j)=NBR_temp;


end

end
end

% Site 84 (Stormandebo)
display('Site 84');

for i=84  % Folder tick

if (i<=72||i>=74)
Path=['/Users/joeaton/Desktop/MatLab modelling/Masterthesis/500x500_17/Site17_',num2str(i)];   % Folder path to where the data is stored
File=dir(fullfile(Path,'*.tif'));              % Open the .tif ending files
FileNames={File.name}';                        % Rename and locates it in a filename string matrix
leng=size(FileNames,1);                        % Loops through the length of the File matrix
for j= 1:leng
[GISImg_84,Ref84] = geotiffread([Path,'/', cell2mat(FileNames(j))]);                          % Loops through MatLab GEOTiff format
NDVI_temp=(GISImg_84(:,:,8)-GISImg_84(:,:,4))./(GISImg_84(:,:,8)+GISImg_84(:,:,4));     % Calculating the NDVI values
NDVI84_18(:,:,j)=NDVI_temp;                                                              % Stores the NDVI values in 3D

NBR_temp=(GISImg_84(:,:,8)-GISImg_84(:,:,12))./(GISImg_84(:,:,8)+GISImg_84(:,:,12));
NBR84_18(:,:,j)=NBR_temp;
```

```
end

end
end

% Site 86 (Stormandebo)
display('Site 86');

for i=86  % Folder tick

if (i<=72||i>=74)
Path=['/Users/joeaton/Desktop/MatLab modelling/Masterthesis/500x500_17/Site17_',num2str(i)];   % Folder path to where the data is stored
File=dir(fullfile(Path,'*.tif'));               % Open the .tif ending files
FileNames={File.name}';                         % Rename and locates it in a filename string matrix
leng=size(FileNames,1);                         % Loops through the length of the File matrix
for j= 1:leng
[GISImg_86,Ref86] = geotiffread([Path,'/', cell2mat(FileNames(j))]);                          % Loops through MatLab GEOTiff format
NDVI_temp=(GISImg_86(:,:,8)-GISImg_86(:,:,4))./(GISImg_86(:,:,8)+GISImg_86(:,:,4));     % Calculating the NDVI values
NDVI86_18(:,:,j)=NDVI_temp;                                                               % Stores the NDVI values in 3D

NBR_temp=(GISImg_86(:,:,8)-GISImg_86(:,:,12))./(GISImg_86(:,:,8)+GISImg_86(:,:,12));
NBR86_18(:,:,j)=NBR_temp;


end

end
end

% Site 100 (Stormandebo)
display('Site 100');

for i=100 % Folder tick

if (i<=72||i>=74)
Path=['/Users/joeaton/Desktop/MatLab modelling/Masterthesis/500x500_17/Site17_',num2str(i)];   % Folder path to where the data is stored
File=dir(fullfile(Path,'*.tif'));               % Open the .tif ending files
FileNames={File.name}';                         % Rename and locates it in a filename string matrix
leng=size(FileNames,1);                         % Loops through the length of the File matrix
for j= 1:leng
[GISImg_100,Ref100] = geotiffread([Path,'/', cell2mat(FileNames(j))]);                          % Loops through MatLab GEOTiff format
NDVI_temp=(GISImg_100(:,:,8)-GISImg_100(:,:,4))./(GISImg_100(:,:,8)+GISImg_100(:,:,4));     % Calculating the NDVI values
NDVI100_18(:,:,j)=NDVI_temp;                                                                  % Stores the NDVI values in 3D

NBR_temp=(GISImg_100(:,:,8)-GISImg_100(:,:,12))./(GISImg_100(:,:,8)+GISImg_100(:,:,12));
NBR100_18(:,:,j)=NBR_temp;


end

end
end
```

```
%% dNBR Processing and viewing

display('dNBR processing')

dNBR_72= (NBR72_17(:,:,7)) - (NBR72_19(:,:,8)); % dNBR calculation using images in the end of the season.

L = zeros(size(dNBR_86)); % Classifies the pixels into categories.
L(dNBR_86>= 0.6) = 1;

L(dNBR_86>= 0.4 & dNBR_86< 0.6) = 2;
L(dNBR_86>= 0.2 & dNBR_86< 0.4) = 3;
L(dNBR_86< 0.2) = 4;

cmap = [1 0 0; 1 1 0; 0 0 1; 0 1 0];

dNBRimage = labeloverlay(dNBR_86,L,'Colormap',cmap); % Creates the new image.

% Figure creation

% First images shows the unclassified image.

figure(1)
subplot(1,2,1)
dNBR_86 = uint8(rescale(dNBR_86, 0, 255));
imshow(dNBR_86,'Colormap',summer)

hold on
title('dNBR for 2018 fire in Stormandebo');
set(gcf, 'color', '#FFFFFF');
plot(55,111,'.','MarkerSize',20,'color','#000000')
plot(55,106,'*','MarkerSize',20,'color','#000000')% Marker to visulize the middle of the plot
legend('Burned', 'Control');
axis on
grid on
ax = gca;
ax.FontSize = 16;
ax.FontWeight = 'bold';
set(gca, 'FontName', 'Times New Roman')
xticks([0:37.3333:112]);
xticklabels({'16.2986^o E','16.3045^o E','16.3105^o E'});
yticks([0:26.5000:212]);
yticklabels({'57.7565^o N','57.7541^o N','','57.7494^o N','','57.7448^o N','','57.7401^o N',''});
c = colorbar;
c.Ticks = ([0:63.75:255])
c.TickLabels = {'Unburned','Low','Moderate','High','High Severity'};
c.Label.String = 'dNBR';
hold off
```

```
% Classified image.

subplot(1,2,2)
imshow(dNBRimage);
hold on
title('dNBR for 2018 fire in Stormandebo');
set(gcf, 'color', '#FFFFFF');
xticks([0:37.3333:112]);
xticklabels({'16.2986^o E','16.3045^o E','16.3105^o E'});
yticks([0:26.5000:212]);
yticklabels({'57.7565^o N','57.7541^o N','','57.7494^o N','','57.7448^o N','','57.7401^o N',''});
plot(55,111,'.','MarkerSize',20,'color','#000000')
plot(55,106,'*','MarkerSize',20,'color','#000000')
legend('Burned', 'Control');
axis on
grid on
annotation('rectangle',[0.87 0.37 0.03 0.03],'Color',[1 0 0],'FaceColor',[1 0 0]);
annotation('rectangle',[0.87 0.32 0.03 0.03],'Color',[1 1 0],'FaceColor',[1 1 0]);
annotation('rectangle',[0.87 0.27 0.03 0.03],'Color',[0 0 1],'FaceColor',[0 0 1]);
annotation('rectangle',[0.87 0.22 0.03 0.03],'Color',[0 1 0],'FaceColor',[0 1 0]);
annotation('textbox',[0.9 0.34 0.9 0.05],'EdgeColor','None','String','High ≥ 0.6','FontName', 'Times New Roman', 'FontSize', 16,'FontWeight','bold');
annotation('textbox',[0.9 0.29 0.9 0.05],'EdgeColor','None','String','Moderate 0.6 < ≥ 0.4','FontName', 'Times New Roman', 'FontSize', 16,'FontWeight','bold');
annotation('textbox',[0.9 0.24 0.9 0.05],'EdgeColor','None','String','Low 0.4 < ≥ 0.2','FontName', 'Times New Roman', 'FontSize', 16,'FontWeight','bold');
annotation('textbox',[0.9 0.19 0.9 0.05],'EdgeColor','None','String','Unburned < 0.2','FontName', 'Times New Roman', 'FontSize', 16,'FontWeight','bold');
ax = gca;
ax.FontSize = 16;
ax.FontWeight = 'bold';
set(gca, 'FontName', 'Times New Roman')
hold off
```

```
%% dNDVI processing and viewing

display('NDVI Processing')

pNDVI_86_1 = (((NDVI86_17(:,:,8)) - (NDVI86_18(:,:,22)))); % dNDVI calculation using images in July for 2017 and 2018.


L = zeros(size(pNDVI_86_1)); % Classifies the pixels into categories.
L(pNDVI_86_1>= 0.3) = 1;
L(pNDVI_86_1>= 0.2 & pNDVI_86_1< 0.3) = 2;
L(pNDVI_86_1>= 0 & pNDVI_86_1< 0.2) = 3;
L(pNDVI_86_1<= 0) = 4;

cmap = [1 0 0; 1 1 0; 0 0 1; 0 1 0];

pNDVIimage1 = labeloverlay(pNDVI_86_1,L,'Colormap',cmap);  % Creates the new image.

pNDVI_86_2 = (((NDVI86_17(:,:,8)) - (NDVI86_21(:,:,8)))); % dNDVI calculation using images in July for 2017 and 2021.


L = zeros(size(pNDVI_86_2)); % Classifies the pixels into categories.
L(pNDVI_86_2>= 0.3) = 1;
L(pNDVI_86_2>= 0.2 & pNDVI_86_2< 0.3) = 2;
L(pNDVI_86_2>= 0 & pNDVI_86_2< 0.2) = 3;
L(pNDVI_86_2<= 0) = 4;

cmap = [1 0 0; 1 1 0; 0 0 1; 0 1 0];

pNDVIimage2 = labeloverlay(pNDVI_86_2,L,'Colormap',cmap);  % Creates the new image.

% Creation of the areal photography.

A = Image_Site_2021;
RGBImage  = A(:,:,[4 3 2]);
RGBImage = uint8(rescale(RGBImage, 0, 255));


figure(2)
% dNDVI 2017-2018

subplot(1,2,1)
imshow(pNDVIimage1);
hold on
title('dNDVI between 2018 and 2017 for Stormandebo');
set(gcf, 'color', '#FFFFFF');
xticks([0:37.3333:112]);
xticklabels({'16.2986^o E','16.3045^o E','16.3105^o E'});
yticks([0:26.5000:212]);
yticklabels({'57.7565^o N','57.7541^o N','','57.7494^o N','','57.7448^o N','','57.7401^o N',''});
plot(55,111,'.','MarkerSize',20,'color','#FDCB59')
plot(55,106,'*','MarkerSize',20,'color','#FDCB59')
legend('Burned', 'Control');
axis on
grid on
annotation('rectangle',[0.43 0.37 0.03 0.03],'Color',[1 0 0],'FaceColor',[1 0 0]);
annotation('rectangle',[0.43 0.32 0.03 0.03],'Color',[1 1 0],'FaceColor',[1 1 0]);
annotation('rectangle',[0.43 0.27 0.03 0.03],'Color',[0 0 1],'FaceColor',[0 0 1]);
annotation('rectangle',[0.43 0.22 0.03 0.03],'Color',[0 1 0],'FaceColor',[0 1 0]);
annotation('textbox',[0.46 0.34 0.9 0.05],'EdgeColor','None','String','No regrowth','FontName', 'Times New Roman', 'FontSize', 16,'FontWeight','bold');
annotation('textbox',[0.46 0.29 0.9 0.05],'EdgeColor','None','String','Low regrowth','FontName', 'Times New Roman', 'FontSize', 16,'FontWeight','bold');
annotation('textbox',[0.46 0.24 0.9 0.05],'EdgeColor','None','String','Moderate regrowth','FontName', 'Times New Roman', 'FontSize', 16,'FontWeight','bold');
annotation('textbox',[0.46 0.19 0.9 0.05],'EdgeColor','None','String','Regrowth','FontName', 'Times New Roman', 'FontSize', 16,'FontWeight','bold');
ax = gca;
ax.FontSize = 16;
set(gca, 'FontName', 'Times New Roman')
hold off

% dNDVI 2017-2021

subplot(1,2,2)
imshow(pNDVIimage2);
hold on
title('dNDVI change between 2021 and 2017 for Stormandebo');
set(gcf, 'color', '#FFFFFF');
xticks([0:37.3333:112]);
xticklabels({'16.2986^o E','16.3045^o E','16.3105^o E'});
yticks([0:26.5000:212]);
yticklabels({'57.7565^o N','57.7541^o N','','57.7494^o N','','57.7448^o N','','57.7401^o N',''});
plot(55,111,'.','MarkerSize',20,'color','#FDCB59')
plot(55,106,'*','MarkerSize',20,'color','#FDCB59')
legend('Burned', 'Control');
axis on
grid on
annotation('rectangle',[0.87 0.37 0.03 0.03],'Color',[1 0 0],'FaceColor',[1 0 0]);
annotation('rectangle',[0.87 0.32 0.03 0.03],'Color',[1 1 0],'FaceColor',[1 1 0]);
annotation('rectangle',[0.87 0.27 0.03 0.03],'Color',[0 0 1],'FaceColor',[0 0 1]);
annotation('rectangle',[0.87 0.22 0.03 0.03],'Color',[0 1 0],'FaceColor',[0 1 0]);
annotation('textbox',[0.9 0.34 0.9 0.05],'EdgeColor','None','String','No regrowth','FontName', 'Times New Roman', 'FontSize', 16,'FontWeight','bold');
annotation('textbox',[0.9 0.29 0.9 0.05],'EdgeColor','None','String','Low regrowth','FontName', 'Times New Roman', 'FontSize', 16,'FontWeight','bold');
annotation('textbox',[0.9 0.24 0.9 0.05],'EdgeColor','None','String','Moderate regrowth','FontName', 'Times New Roman', 'FontSize', 16,'FontWeight','bold');
annotation('textbox',[0.9 0.19 0.9 0.05],'EdgeColor','None','String','Regrowth','FontName', 'Times New Roman', 'FontSize', 16,'FontWeight','bold');
ax = gca;
ax.FontSize = 16;
set(gca, 'FontName', 'Times New Roman')
hold off
```

```
%% Arial photo
```

```
f = figure;

figure(f)
imshow(RGBImage);
hold on
title('Areial photo of Stormandebo 2021');
set(gcf, 'color', '#FFFFFF');
xticks([0:37.3333:112]);
xticklabels({'16.2986^o E','16.3045^o E','16.3105^o E'});
yticks([0:26.5000:212]);
yticklabels({'57.7565^o N','57.7541^o N','','57.7494^o N','','57.7448^o N','','57.7401^o N',''});
plot(55,111,'.','MarkerSize',20,'color','#DA0A0A')
plot(55,106,'*','MarkerSize',20,'color','#5FDA0A')
legend('Burned', 'Control');
axis on
grid on
ax = gca;
ax.FontSize = 16;
set(gca, 'FontName', 'Times New Roman')
hold off
```

```
%% ARSTAN Indices extraction

% Importation of data was made through Matlabs own importation function in
% tabs (Variable).

%%%%%%% Extraction of data %%%%%%%%%%

display('ARSTAN Indices')

% Renaming the imported sheets

Kil_B = TreeCoreData;
Kil_C = TreeCoreDataS1;

Lessebo_B = TreeCoreDataS2;
Lessebo_C = TreeCoreDataS3;

Osterby_B = TreeCoreDataS4;
Osterby_C = TreeCoreDataS5;

Rullerum_B = TreeCoreDataS6;
Rullerum_C = TreeCoreDataS7;

Storm_B = TreeCoreDataS8;
Storm_C = TreeCoreDataS9;

Kil_B = Kil_B(:,8);
Kil_C = Kil_C(:,8);

Lessebo_B = Lessebo_B(:,8);
Lessebo_C = Lessebo_C(:,8);

Osterby_B = Osterby_B(:,8);
Osterby_C = Osterby_C(:,8);

Rullerum_B = Rullerum_B(:,8);
Rullerum_C = Rullerum_C(:,8);

Storm_B = Storm_B(:,8);
Storm_C = Storm_C(:,8);

% Extracting values from 2010 - 2021

TW_72_B = Kil_B(94:104,:);
TW_72_C = Kil_C(101:111,:);

TW_82_B = Rullerum_B(97:107,:);
TW_82_C = Rullerum_C(221:231,:);

TW_84_B = Osterby_B(32:42,:);
TW_84_C = Osterby_C(15:25,:);

TW_86_B = Storm_B(104:114,:);
TW_86_C = Storm_C(104:114,:);

TW_100_B = Lessebo_B(46:56,:);
TW_100_C = Lessebo_C(66:76,:);

% Calculationg the ratio of growth from the ARSTAN Indices, the mean value
% between 2010-2017 was extracted. The ratio is calculated by taking the
% value of intrest and divided by the mean value.

 TW_72_B_R(1,:) = mean(TW_72_B(1:7,:));
 TW_72_B_R(2,:) = (TW_72_B(8,:))/(TW_72_B_R(1,:));
 TW_72_B_R(3,:) = (TW_72_B(9,:))/(TW_72_B_R(1,:));
 TW_72_B_R(4,:) = (TW_72_B(10,:))/(TW_72_B_R(1,:));
 TW_72_B_R(5,:) = (TW_72_B(11,:))/(TW_72_B_R(1,:));

 TW_B2021= [TW_72_B_R(5,:) TW_82_B_R(5,:) TW_84_B_R(5,:) TW_86_B_R(5,:) TW_100_B_R(5,:)]'
 TW_C2021= [TW_72_C_R(5,:) TW_82_C_R(5,:) TW_84_C_R(5,:) TW_86_C_R(5,:) TW_100_C_R(5,:)]'

 % Standard deviation for ARSTAN Indices

 TW_SB2020 = std(TW_B2020);
 TW_SC2020 = std(TW_C2020);
```

```
%% Statistics (1/4)

%%%%%%%% Extraction of the mean value and standard deviation for dNBR %%%%%%%%%%

% dNBR Burn plot
```

```
display('dNBR Burn plot')

dNBR_72_B = mean(mean(dNBR_72(148:150,72:74)));

dNBR_82_B = mean(mean(dNBR_82(148:150,80:82)));

dNBR_84_B = mean(mean(dNBR_84(148:150,84:86)));

dNBR_86_B = mean(mean(dNBR_86(110:112,54:56)));

dNBR_100_B = mean(mean(dNBR_100(154:156,99:101)));

dNBR_B = [dNBR_72_B dNBR_82_B dNBR_84_B dNBR_86_B dNBR_100_B]';
dNBR_SB = std(dNBR_B);

% dNBR Control plot

display('dNBR Control plot')

dNBR_72_C = mean(mean(dNBR_72(156:158,80:81)));

dNBR_82_C = mean(mean(dNBR_82(158:160,81:83)));

dNBR_84_C = mean(mean(dNBR_84(156:158,81:83)));

dNBR_86_C = mean(mean(dNBR_86(105:107,54:56)));

dNBR_100_C = mean(mean(dNBR_100(155:158,82:84)));

dNBR_C = [dNBR_72_C dNBR_82_C dNBR_84_C dNBR_86_C dNBR_100_C]';
dNBR_SC = std(dNBR_C);

% dNBR Center Burn plot

display('dNBR Center Burn plot')

dNBR_72_M = mean(mean(dNBR_72(143:145,66:68)));

dNBR_82_M = mean(mean(dNBR_82(147:149,81:83)));

dNBR_84_M = mean(mean(dNBR_84(149:151,83:85)));

dNBR_86_M = mean(mean(dNBR_86(113:115,59:61)));

dNBR_100_M = mean(mean(dNBR_100(147:149,115:117)));

dNBR_M = [dNBR_72_M dNBR_82_M dNBR_84_M dNBR_86_M dNBR_100_M]';
dNBR_SM = std(dNBR_M);
```

```
%% Statistics (2/4)

%%%%%%%% Extraction of the mean value and standard deviation for NDVI %%%%%%%%%%

% NDVI Burn plot

display('NDVI Burn plot')

NDVI_72_B = mean(mean(NDVI72_21(148:150,72:74)));

NDVI_82_B = mean(mean(NDVI82_21(148:150,80:82)));

NDVI_84_B = mean(mean(NDVI84_21(148:150,84:86)));

NDVI_86_B = mean(mean(NDVI86_21(110:112,54:56)));

NDVI_100_B = mean(mean(NDVI100_21(154:156,99:101)));

NDVI_B21 = [NDVI_72_B NDVI_82_B NDVI_84_B NDVI_86_B NDVI_100_B]';
NDVI_SB21 = std(NDVI_B21);

% NDVI Control plot

display('NDVI Control plot')

NDVI_72_C = mean(mean(NDVI72_21(156:158,80:81)));

NDVI_82_C = mean(mean(NDVI82_21(158:160,81:83)));

NDVI_84_C = mean(mean(NDVI84_21(156:158,81:83)));

NDVI_86_C = mean(mean(NDVI86_21(105:107,54:56)));

NDVI_100_C = mean(mean(NDVI100_21(155:158,82:84)));

NDVI_C21 = [NDVI_72_C NDVI_82_C NDVI_84_C NDVI_86_C NDVI_100_C]';
NDVI_SC21 = std(NDVI_C21);
```

```
% NDVI Center Burn plot

display('NDVI Center Burn plot')

NDVI_72_M = mean(mean(NDVI72_21(143:145,66:68)));

NDVI_82_M = mean(mean(NDVI82_21(147:149,81:83)));

NDVI_84_M = mean(mean(NDVI84_21(149:151,83:85)));

NDVI_86_M = mean(mean(NDVI86_21(113:115,59:61)));

NDVI_100_M = mean(mean(NDVI100_21(147:149,115:117)));

NDVI_M21 = [NDVI_72_M NDVI_82_M NDVI_84_M NDVI_86_M NDVI_100_M]';
```

```
%% Statistics (3/4)

%%%%%%%% Variance calculation %%%%%%%%%

% dNBR Variance
display('dNBR Variance')

dNBR_B_V = var(dNBR_B);
dNBR_C_V = var(dNBR_C);
dNBR_M_V = var(dNBR_M);

Variance_dNBR = [dNBR_B_V dNBR_C_V dNBR_M_V];

% NDVI Variance
display('NDVI Variance')

% Burned
NDVI_B17_V = var(NDVI_B17)
NDVI_B18_V = var(NDVI_B18)
NDVI_B19_V = var(NDVI_B19)
NDVI_B20_V = var(NDVI_B20)
NDVI_B21_V = var(NDVI_B21)

Variance_NDVI_Burned = [NDVI_B17_V NDVI_B18_V NDVI_B19_V NDVI_B20_V NDVI_B21_V];

% Control
NDVI_C17_V = var(NDVI_C17)
NDVI_C18_V = var(NDVI_C18)
NDVI_C19_V = var(NDVI_C19)
NDVI_C20_V = var(NDVI_C20)
NDVI_C21_V = var(NDVI_C21)

Variance_NDVI_Control = [NDVI_C17_V NDVI_C18_V NDVI_C19_V NDVI_C20_V NDVI_C21_V];

% ARSTAN Indices Variance
display('ARSTAN Variance')

% Burned
TW_B2017_V = var(TW_B2017)
TW_B2018_V = var(TW_B2018)
TW_B2019_V = var(TW_B2019)
TW_B2020_V = var(TW_B2020)
TW_B2021_V = var(TW_B2021)

Variance_ARSTAN_Burned = [TW_B2017_V TW_B2018_V TW_B2019_V TW_B2020_V TW_B2021_V];

% Control
TW_C2017_V = var(TW_C2017)
TW_C2018_V = var(TW_C2018)
TW_C2019_V = var(TW_C2019)
TW_C2020_V = var(TW_C2020)
TW_C2021_V = var(TW_C2021)

Variance_ARSTAN_Control = [TW_C2017_V TW_C2018_V TW_C2019_V TW_C2020_V TW_C2021_V];

%%%%%%%% Mean calculation %%%%%%%%%%

% dNBR Mean
display('dNBR Mean')

dNBR_B_M = mean(dNBR_B);
dNBR_C_M = mean(dNBR_C);
dNBR_M_M = mean(dNBR_M);

Mean_dNBR = [dNBR_B_M dNBR_C_M dNBR_M_M];
```

```
% NDVI mean
display('NDVI Mean')

% Control
NDVI_C17_M = mean(NDVI_C17)
NDVI_C18_M = mean(NDVI_C18)
NDVI_C19_M = mean(NDVI_C19)
NDVI_C20_M = mean(NDVI_C20)
NDVI_C21_M = mean(NDVI_C21)

% Burned
NDVI_B17_M = mean(NDVI_B17)
NDVI_B18_M = mean(NDVI_B18)
NDVI_B19_M = mean(NDVI_B19)
NDVI_B20_M = mean(NDVI_B20)
NDVI_B21_M = mean(NDVI_B21)

% ARSTAN indices
display('ARSTAN Mean')

% Control
TW_C2017_M = mean(TW_C2017)
TW_C2018_M = mean(TW_C2018)
TW_C2019_M = mean(TW_C2019)
TW_C2020_M = mean(TW_C2020)
TW_C2021_M = mean(TW_C2021)

Mean_ARSTAN_Control = [TW_C2017_M TW_C2018_M TW_C2019_M TW_C2020_M TW_C2021_M];

% Burned
TW_B2017_M = mean(TW_B2017)
TW_B2018_M = mean(TW_B2018)
TW_B2019_M = mean(TW_B2019)
TW_B2020_M = mean(TW_B2020)
TW_B2021_M = mean(TW_B2021)

Mean_ARSTAN_Burned = [TW_B2017_M TW_B2018_M TW_B2019_M TW_B2020_M TW_B2021_M];
```

```
%% Statistics (4/4)

%%%%%%% Box plot of dNBR %%%%%%%%%

A = dNBR_B;
B = dNBR_C;
C = dNBR_M;

group = [ones(size(A));
    2 * ones(size(B));
    3 * ones(size(C))];

for i = 1:length(group(:,1))

    if group(i) == 1
        group(i) = Variance_dNBR(:,1);
    else
        group(i) = group(i);

        if group(i) == 2
                group(i) = Variance_dNBR(:,2)

           else
               group(i) = group(i);

               if group(i) == 3
                   group(i) = Variance_dNBR(:,3)
               else
                   group(i) = group(i);
               end

           end
       end
end

figure(4)
hold on
title('Mean dNBR against dNBR variance','FontSize', 22,'FontWeight','bold')
boxplot([A, B, C],group);
xlabel('Variance','FontWeight','bold');
ylabel('Mean','FontWeight','bold');
set(gca, 'FontName', 'Times New Roman','FontSize', 22)
set(gcf, 'color', '#FFFFFF');
```

```
%%%%%% Permutation test %%%%%%%%%

% This subsection is where the Permutation test is conducted:
% Input values, first "Sample" then "Control"

display('Permutation test')

[p, observeddifference, effectsize] = permutationTest(NDVI_B21, NDVI_C21, 1000, 'plotresult',1)

%%%%% Scatter plot %%%%%%%%%%

% dNBR vs. Arstan indices

figure(5)
hold on
title('dNBR values against ARSTAN indices 2019','FontSize', 22,'FontWeight','bold')
xlabel('dNBR','FontSize', 22,'FontWeight','bold')
ylabel('ARSTAN Indices','FontSize', 22,'FontWeight','bold')
plot(dNBR_B, TW_B2019,'.','MarkerSize',20,'color','#D91111')
plot(dNBR_C, TW_C2019,'*','MarkerSize',20,'color','#4A9012')
plot(dNBR_M, TW_B2019,'+','MarkerSize',20,'color','#D91111')
legend('Burned', 'Control', 'Middel Burn plot')
set(gca, 'FontName', 'Times New Roman','FontSize', 22)
set(gcf, 'color', '#FFFFFF');

%%%%%% Correlation Coefficient %%%%%%

R1 = corrcoef(dNBR_B, TW_B2018);
R2 = corrcoef(dNBR_B, TW_B2019);
R3 = corrcoef(dNBR_M, TW_B2018);
```

```
%% NDVI Subplots

% Correlation between NDVI and ARSTAN Indices

%%%%%%%% Extracting Site values %%%%%%%%%%%%

Kil_NDVI_B = [(NDVI_B17(1,:)) (NDVI_B18(1,:)) (NDVI_B19(1,:)) (NDVI_B20(1,:)) (NDVI_B21(1,:))]';
Kil_NDVI_C = [(NDVI_C17(1,:)) (NDVI_C18(1,:)) (NDVI_C19(1,:)) (NDVI_C20(1,:)) (NDVI_C21(1,:))]';

Kil_TW_B = [(TW_B2017(1,:)) (TW_B2018(1,:)) (TW_B2019(1,:)) (TW_B2020(1,:)) (TW_B2021(1,:))]';
Kil_TW_C = [(TW_C2017(1,:)) (TW_C2018(1,:)) (TW_C2019(1,:)) (TW_C2020(1,:)) (TW_C2021(1,:))]';

Rullerum_NDVI_B = [(NDVI_B17(2,:)) (NDVI_B18(2,:)) (NDVI_B19(2,:)) (NDVI_B20(2,:)) (NDVI_B21(2,:))]';
Rullerum_NDVI_C = [(NDVI_C17(2,:)) (NDVI_C18(2,:)) (NDVI_C19(2,:)) (NDVI_C20(2,:)) (NDVI_C21(2,:))]';

Rullerum_TW_B = [(TW_B2017(2,:)) (TW_B2018(2,:)) (TW_B2019(2,:)) (TW_B2020(2,:)) (TW_B2021(2,:))]';
Rullerum_TW_C = [(TW_C2017(2,:)) (TW_C2018(2,:)) (TW_C2019(2,:)) (TW_C2020(2,:)) (TW_C2021(2,:))]';

Osterbymo_NDVI_B = [(NDVI_B17(3,:)) (NDVI_B18(3,:)) (NDVI_B19(3,:)) (NDVI_B20(3,:)) (NDVI_B21(3,:))]';
Osterbymo_NDVI_C = [(NDVI_C17(3,:)) (NDVI_C18(3,:)) (NDVI_C19(3,:)) (NDVI_C20(3,:)) (NDVI_C21(3,:))]';

Osterbymo_TW_B = [(TW_B2017(3,:)) (TW_B2018(3,:)) (TW_B2019(3,:)) (TW_B2020(3,:)) (TW_B2021(3,:))]';
Osterbymo_TW_C = [(TW_C2017(3,:)) (TW_C2018(3,:)) (TW_C2019(3,:)) (TW_C2020(3,:)) (TW_C2021(3,:))]';

Stormandebo_NDVI_B = [(NDVI_B17(4,:)) (NDVI_B18(4,:)) (NDVI_B19(4,:)) (NDVI_B20(4,:)) (NDVI_B21(4,:))]';
Stormandebo_NDVI_C = [(NDVI_C17(4,:)) (NDVI_C18(4,:)) (NDVI_C19(4,:)) (NDVI_C20(4,:)) (NDVI_C21(4,:))]';

Stormandebo_TW_B = [(TW_B2017(4,:)) (TW_B2018(4,:)) (TW_B2019(4,:)) (TW_B2020(4,:)) (TW_B2021(4,:))]';
Stormandebo_TW_C = [(TW_C2017(4,:)) (TW_C2018(4,:)) (TW_C2019(4,:)) (TW_C2020(4,:)) (TW_C2021(4,:))]';

Lessebo_NDVI_B = [(NDVI_B17(5,:)) (NDVI_B18(5,:)) (NDVI_B19(5,:)) (NDVI_B20(5,:)) (NDVI_B21(5,:))]';
Lessebo_NDVI_C = [(NDVI_C17(5,:)) (NDVI_C18(5,:)) (NDVI_C19(5,:)) (NDVI_C20(5,:)) (NDVI_C21(5,:))]';

Lessebo_TW_B = [(TW_B2017(5,:)) (TW_B2018(5,:)) (TW_B2019(5,:)) (TW_B2020(5,:)) (TW_B2021(5,:))]';
Lessebo_TW_C = [(TW_C2017(5,:)) (TW_C2018(5,:)) (TW_C2019(5,:)) (TW_C2020(5,:)) (TW_C2021(5,:))]';

%%%%%%%%% Subplots %%%%%%%%%

figure(6)
```

```
% Kil

subplot(3,2,1)
hold on
title('NDVI values against ARSTAN indices for Kil','FontSize', 22,'FontWeight','bold')
xlabel('Year','FontSize', 22,'FontWeight','bold')
set(gca, 'FontName', 'Times New Roman','FontSize', 22)
set(gcf, 'color', '#FFFFFF');
yyaxis left
ylabel('NDVI','FontSize', 22,'FontWeight','bold')
plot(Year,Kil_NDVI_B,'--','color','#E64D1C','LineWidth',3)
plot(Year,Kil_NDVI_C,'-.','color','#4A9012','LineWidth',3)
set(gca,'ycolor','#000000')
yyaxis right
ylabel('ARSTAN Indices','FontSize', 22,'FontWeight','bold')
plot(Year,Kil_TW_B,':','color','#E64D1C','LineWidth',3)
plot(Year,Kil_TW_C,'-','color','#4A9012','LineWidth',3)
set(gca,'ycolor','#000000')
legend('NDVI Burned', 'NDVI Control', 'ARSTAN indices Burned', 'ARSTAN indices Control')

% Rullerum

subplot(3,2,2)
hold on
title('NDVI values against ARSTAN indices for Rullerum','FontSize', 22,'FontWeight','bold')
xlabel('Year','FontSize', 22,'FontWeight','bold')
set(gca, 'FontName', 'Times New Roman','FontSize', 22)
set(gcf, 'color', '#FFFFFF');
yyaxis left
ylabel('NDVI','FontSize', 22,'FontWeight','bold')
plot(Year,Rullerum_NDVI_B,'--','color','#E64D1C','LineWidth',3)
plot(Year,Rullerum_NDVI_C,'-.','color','#4A9012','LineWidth',3)
set(gca,'ycolor','#000000')
yyaxis right
ylabel('ARSTAN Indices','FontSize', 22,'FontWeight','bold')
plot(Year,Rullerum_TW_B,':','color','#E64D1C','LineWidth',3)
plot(Year,Rullerum_TW_C,'-','color','#4A9012','LineWidth',3)
set(gca,'ycolor','#000000')

% Österbymo

subplot(3,2,3)
hold on
title('NDVI values against ARSTAN indices for Österbymo','FontSize', 22,'FontWeight','bold')
xlabel('Year','FontSize', 22,'FontWeight','bold')
set(gca, 'FontName', 'Times New Roman','FontSize', 22)
set(gcf, 'color', '#FFFFFF');
yyaxis left
ylabel('NDVI','FontSize', 22,'FontWeight','bold')
plot(Year,Osterbymo_NDVI_B,'--','color','#E64D1C','LineWidth',3)
plot(Year,Osterbymo_NDVI_C,'-.','color','#4A9012','LineWidth',3)
set(gca,'ycolor','#000000')
yyaxis right
ylabel('ARSTAN Indices','FontSize', 22,'FontWeight','bold')
plot(Year,Osterbymo_TW_B,':','color','#E64D1C','LineWidth',3)
plot(Year,Osterbymo_TW_C,'-','color','#4A9012','LineWidth',3)
set(gca,'ycolor','#000000')

% Stormandebo

subplot(3,2,4)
hold on
title('NDVI values against ARSTAN indices for Stormandebo','FontSize', 22,'FontWeight','bold')
xlabel('Year','FontSize', 22,'FontWeight','bold')
set(gca, 'FontName', 'Times New Roman','FontSize', 22)
set(gcf, 'color', '#FFFFFF');
yyaxis left
ylabel('NDVI','FontSize', 22,'FontWeight','bold')
plot(Year,Stormandebo_NDVI_B,'--','color','#E64D1C','LineWidth',3)
plot(Year,Stormandebo_NDVI_C,'-.','color','#4A9012','LineWidth',3)
set(gca,'ycolor','#000000')
yyaxis right
ylabel('ARSTAN Indices','FontSize', 22,'FontWeight','bold')
plot(Year,Stormandebo_TW_B,':','color','#E64D1C','LineWidth',3)
plot(Year,Stormandebo_TW_C,'-','color','#4A9012','LineWidth',3)
set(gca,'ycolor','#000000')

% Lessebo

subplot(3,2,5)
hold on
title('NDVI values against ARSTAN indices for Lessebo','FontSize', 22,'FontWeight','bold')
xlabel('Year','FontSize', 22,'FontWeight','bold')
set(gca, 'FontName', 'Times New Roman','FontSize', 22)
set(gcf, 'color', '#FFFFFF');
yyaxis left
ylabel('NDVI','FontSize', 22,'FontWeight','bold')
plot(Year,Lessebo_NDVI_B,'--','color','#E64D1C','LineWidth',3)
plot(Year,Lessebo_NDVI_C,'-.','color','#4A9012','LineWidth',3)
set(gca,'ycolor','#000000')
yyaxis right
ylabel('ARSTAN Indices','FontSize', 22,'FontWeight','bold')
plot(Year,Lessebo_TW_B,':','color','#E64D1C','LineWidth',3)
plot(Year,Lessebo_TW_C,'-','color','#4A9012','LineWidth',3)
set(gca,'ycolor','#000000')
```

Appendix VI: Permutation test in MATLAB

Permutation test provided in MATLAB add on function. This is an automatic function which was applied to test the difference between two samples (one control and one sample) and returns also an effect size. The code is free for download in MATLAB.

```
% [p, observeddifference, effectsize] = permutationTest(sample1, sample2, permutations [, varargin])
%
%       Permutation test (aka randomisation test), testing for a difference
%       in means between two samples.
%
% In:
%       sample1 - vector of measurements from one (experimental) sample
%       sample2 - vector of measurements from a second (control) sample
%       permutations - the number of permutations
%
% Optional (name-value pairs):
%       sidedness - whether to test one- or two-sided:
%           'both' - test two-sided (default)
%           'smaller' - test one-sided, alternative hypothesis is that
%                       the mean of sample1 is smaller than the mean of
%                       sample2
%           'larger' - test one-sided, alternative hypothesis is that
%                      the mean of sample1 is larger than the mean of
%                      sample2
%       exact - whether or not to run an exact test, in which all possible
%               combinations are considered. this is only feasible for
%               relatively small sample sizes. the 'permutations' argument
%               will be ignored for an exact test. (1|0, default 0)
%       plotresult - whether or not to plot the distribution of randomised
%                    differences, along with the observed difference (1|0,
%                    default: 0)
%       showprogress - whether or not to show a progress bar. if 0, no bar
%                      is displayed; if showprogress > 0, the bar updates
%                      every showprogress-th iteration.
%
% Out:
%       p - the resulting p-value
%       observeddifference - the observed difference between the two
%                            samples, i.e. mean(sample1) - mean(sample2)
%       effectsize - the effect size, Hedges' g
%
% Usage example:
%       >> permutationTest(rand(1,100), rand(1,100)-.25, 10000, ...
%          'plotresult', 1, 'showprogress', 250)
%
%                   Copyright 2015-2018, 2021 Laurens R Krol
%                   Team PhyPA, Biological Psychology and Neuroergonomics,
%                   Berlin Institute of Technology


% 2021-01-13 lrk
%   - Replaced effect size calculation with Hedges' g, from Hedges & Olkin
%     (1985), Statistical Methods for Meta-Analysis (p. 78, formula 3),
%     Orlando, FL, USA: Academic Press.
% 2020-07-14 lrk
%   - Added version-dependent call to hist/histogram
% 2019-02-01 lrk
%   - Added short description
%   - Increased the number of bins in the plot
% 2018-03-15 lrk
%   - Suppressed initial MATLAB:nchoosek:LargeCoefficient warning
% 2018-03-14 lrk
%   - Added exact test
% 2018-01-31 lrk
%   - Replaced calls to mean() with nanmean()
% 2017-06-15 lrk
%   - Updated waitbar message in first iteration
% 2017-04-04 lrk
%   - Added progress bar
% 2017-01-13 lrk
%   - Switched to inputParser to parse arguments
% 2016-09-13 lrk
%   - Caught potential issue when column vectors were used
%   - Improved plot
% 2016-02-17 toz
%   - Added plot functionality
% 2015-11-26 First version

% This program is free software: you can redistribute it and/or modify
% it under the terms of the GNU General Public License as published by
% the Free Software Foundation, either version 3 of the License, or
% (at your option) any later version.
%
% This program is distributed in the hope that it will be useful,
% but WITHOUT ANY WARRANTY; without even the implied warranty of
% MERCHANTABILITY or FITNESS FOR A PARTICULAR PURPOSE.  See the
% GNU General Public License for more details.
%
% You should have received a copy of the GNU General Public License
% along with this program.  If not, see <http://www.gnu.org/licenses/>.
```

```
function [p, observeddifference, effectsize] = permutationTest(sample1, sample2, permutations, varargin)

% parsing input
p = inputParser;

addRequired(p, 'sample1', @isnumeric);
addRequired(p, 'sample2', @isnumeric);
addRequired(p, 'permutations', @isnumeric);

addParamValue(p, 'sidedness', 'both', @(x) any(validatestring(x,{'both', 'smaller', 'larger'})));
addParamValue(p, 'exact' , 0, @isnumeric);
addParamValue(p, 'plotresult', 0, @isnumeric);
addParamValue(p, 'showprogress', 0, @isnumeric);

parse(p, sample1, sample2, permutations, varargin{:})

sample1 = p.Results.sample1;
sample2 = p.Results.sample2;
permutations = p.Results.permutations;
sidedness = p.Results.sidedness;
exact = p.Results.exact;
plotresult = p.Results.plotresult;
showprogress = p.Results.showprogress;

% enforcing row vectors
if iscolumn(sample1), sample1 = sample1'; end
if iscolumn(sample2), sample2 = sample2'; end

allobservations = [sample1, sample2];
observeddifference = nanmean(sample1) - nanmean(sample2);
pooledstd = sqrt(  ( (numel(sample1)-1)*std(sample1)^2 + (numel(sample2)-1)*std(sample2)^2 )  /  ( numel(allobservations)-2 )  );
effectsize = observeddifference / pooledstd;

w = warning('off', 'MATLAB:nchoosek:LargeCoefficient');
if ~exact && permutations > nchoosek(numel(allobservations), numel(sample1))
    warning(['the number of permutations (%d) is higher than the number of possible combinations (%d);\n' ...
             'consider running an exact test using the ''exact'' argument'], ...
            permutations, nchoosek(numel(allobservations), numel(sample1)));
end
warning(w);

if showprogress, w = waitbar(0, 'Preparing test...', 'Name', 'permutationTest'); end

if exact
    % getting all possible combinations
    allcombinations = nchoosek(1:numel(allobservations), numel(sample1));
    permutations = size(allcombinations, 1);
end
```

```
% running test
randomdifferences = zeros(1, permutations);
if showprogress, waitbar(0, w, sprintf('Permutation 1 of %d', permutations), 'Name', 'permutationTest'); end
for n = 1:permutations
    if showprogress && mod(n,showprogress) == 0, waitbar(n/permutations, w, sprintf('Permutation %d of %d', n, permutations)); end

    % selecting either next combination, or random permutation
    if exact, permutation = [allcombinations(n,:), setdiff(1:numel(allobservations), allcombinations(n,:))];
    else, permutation = randperm(length(allobservations)); end

    % dividing into two samples
    randomSample1 = allobservations(permutation(1:length(sample1)));
    randomSample2 = allobservations(permutation(length(sample1)+1:length(permutation)));

    % saving differences between the two samples
    randomdifferences(n) = nanmean(randomSample1) - nanmean(randomSample2);
end
if showprogress, delete(w); end

% getting probability of finding observed difference from random permutations
if strcmp(sidedness, 'both')
    p = (length(find(abs(randomdifferences) > abs(observeddifference)))+1) / (permutations+1);
elseif strcmp(sidedness, 'smaller')
    p = (length(find(randomdifferences < observeddifference))+1) / (permutations+1);
elseif strcmp(sidedness, 'larger')
    p = (length(find(randomdifferences > observeddifference))+1) / (permutations+1);
end

% plotting result
if plotresult
    figure;
    if verLessThan('matlab', '8.4')
        % MATLAB R2014a and earlier
        hist(randomdifferences, 20);
    else
        % MATLAB R2014b and later
        histogram(randomdifferences, 20);
    end
    hold on;
    xlabel('Random differences');
    ylabel('Count')
    od = plot(observeddifference, 0, '*r', 'DisplayName', sprintf('Observed difference.\nEffect size: %.2f,\np = %f', effectsize, p));
    legend(od);
end

end
```

Appendix VII: Areal images for all sites year 2021

Areal image (RGB) of the site Kil (72), Rullerum (82), Österbymo (84), Stormandebo (86), and Lessebo (100) year 2021. The red dot (.) corresponds to the burn plot, and the green star (*) corresponds to the control plot. The images also contains the coordinates longitude and latitude.

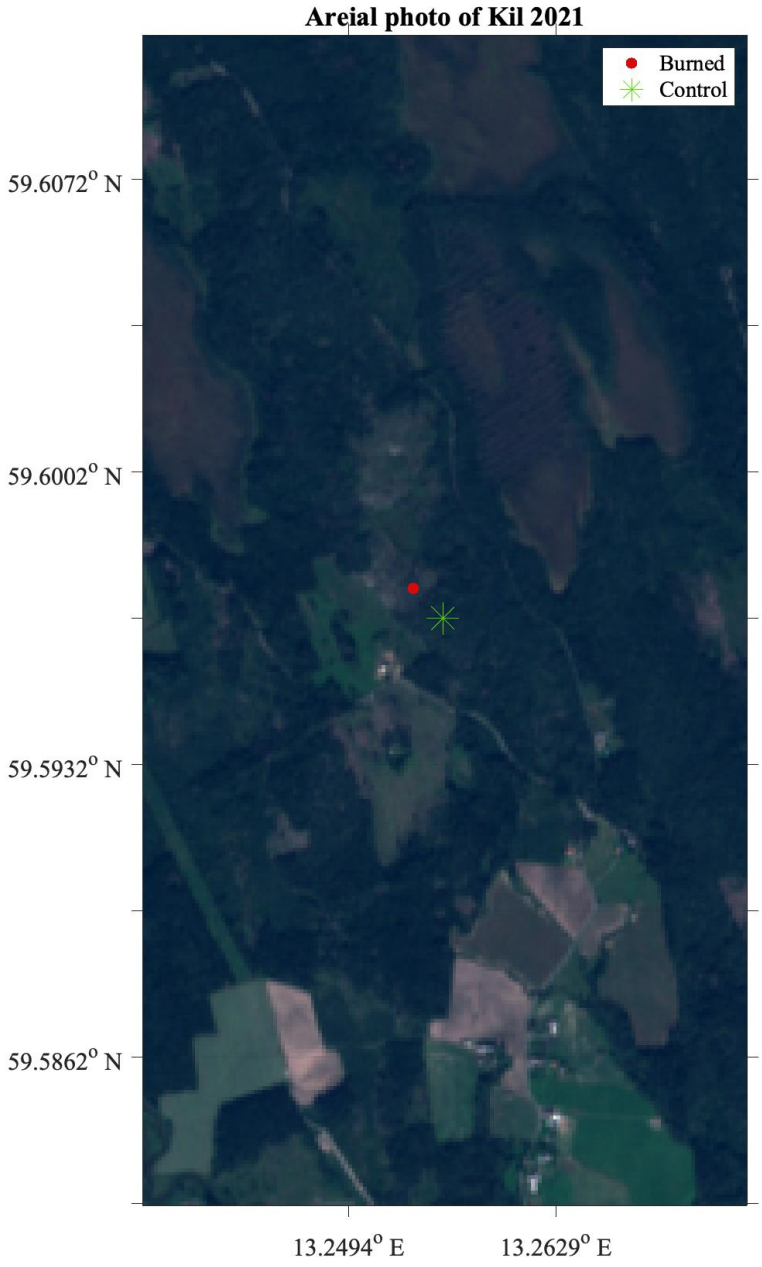

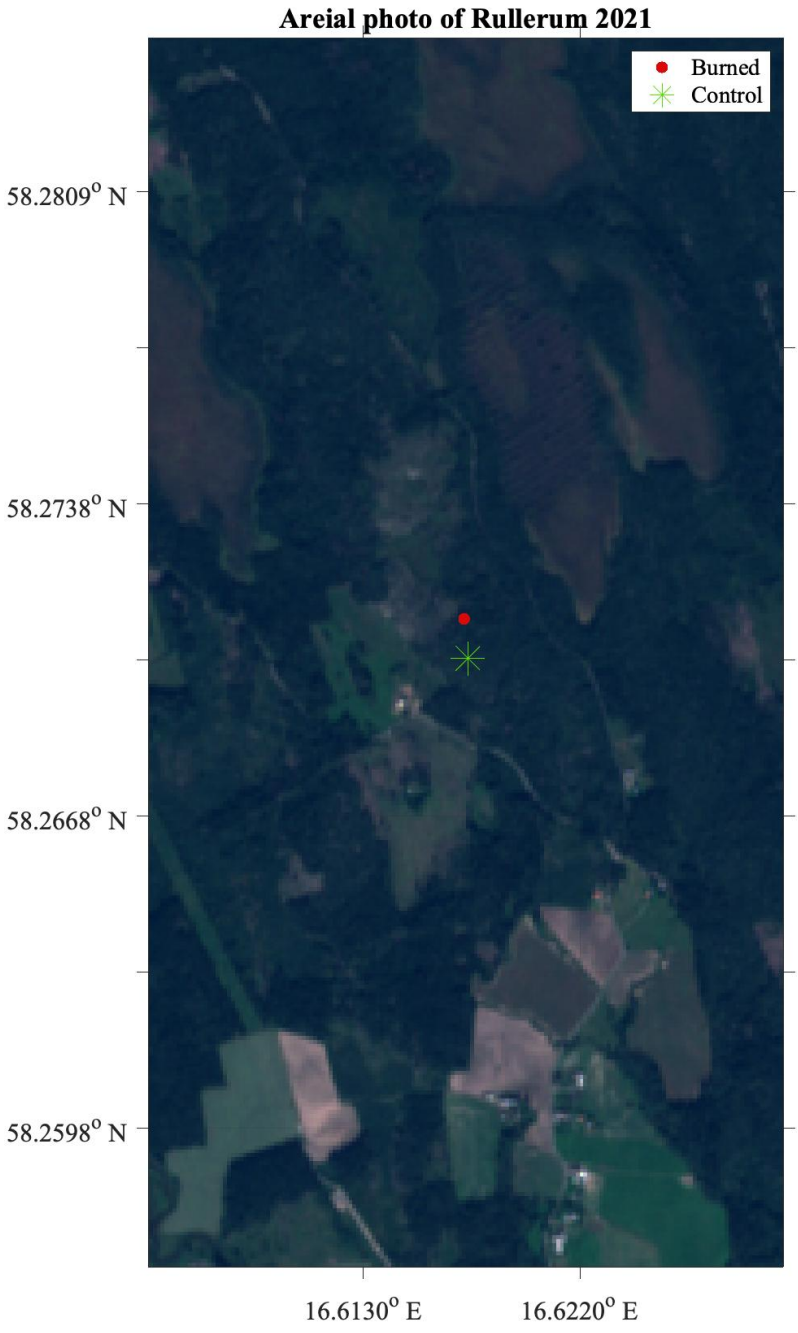
Areial photo of Rullerum 2021
Burned
Control
58.2809° N
58.2738° N
58.2668° N
58.2598° N
16.6130° E
16.6220° E

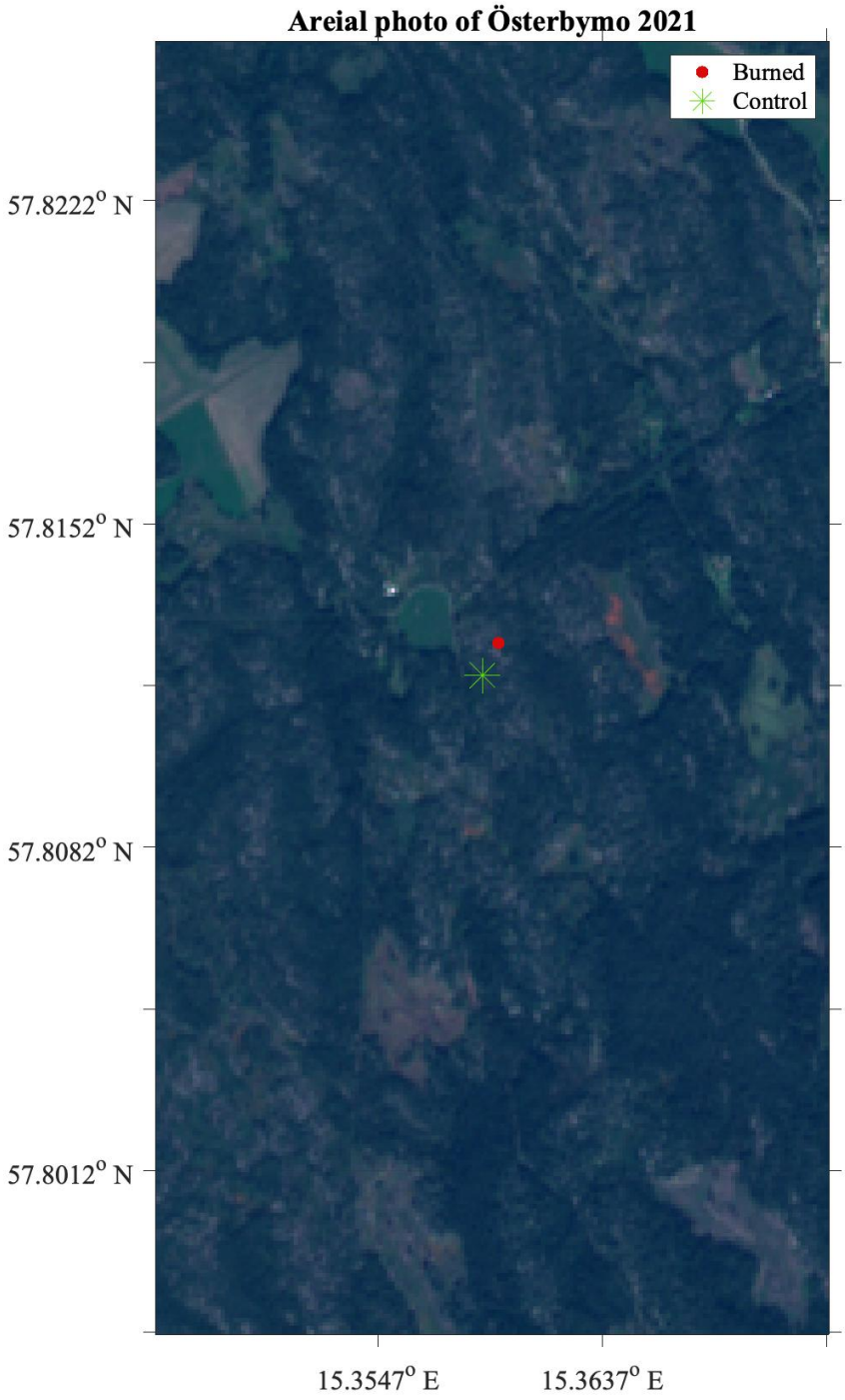
Areial photo of Österbymo 2021
Burned
Control
57.8222° N
57.8152° N
57.8082° N
57.8012° N
15.3547° E
15.3637° E

Areial photo of Stormandebo 2021

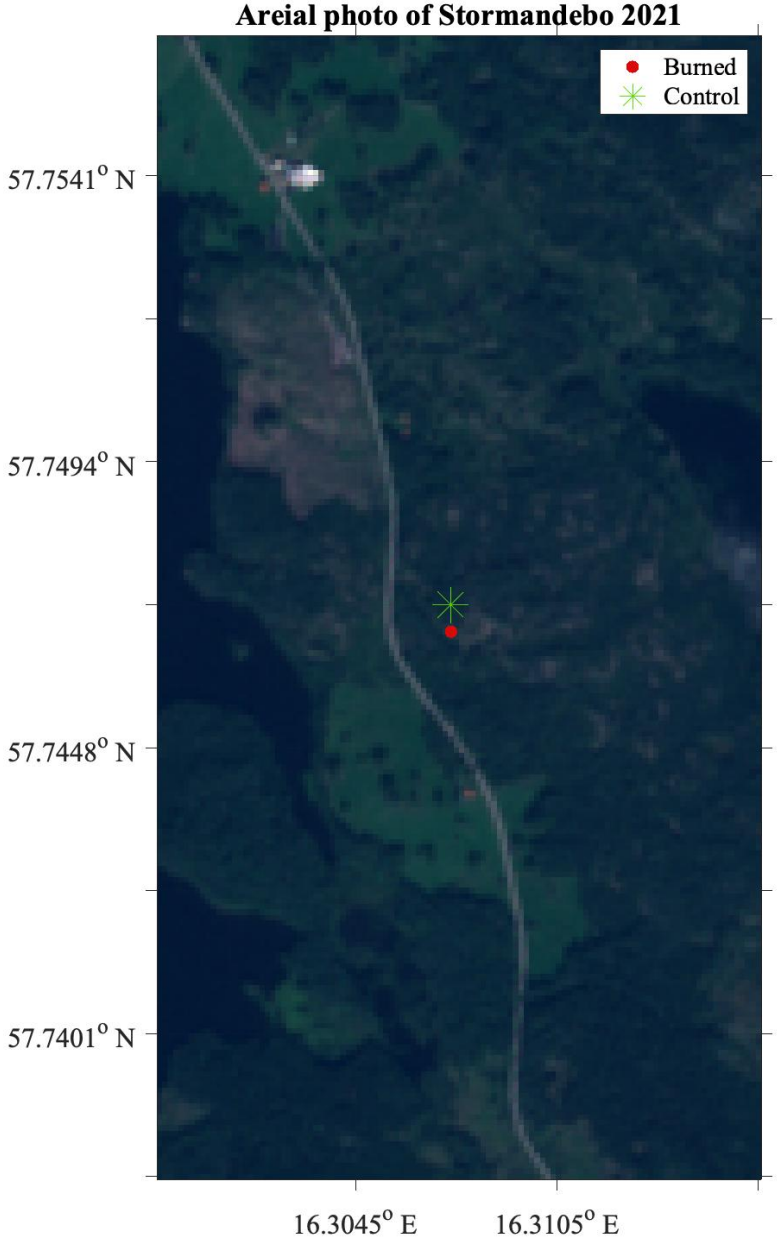

Areial photo of Lessebo 2021

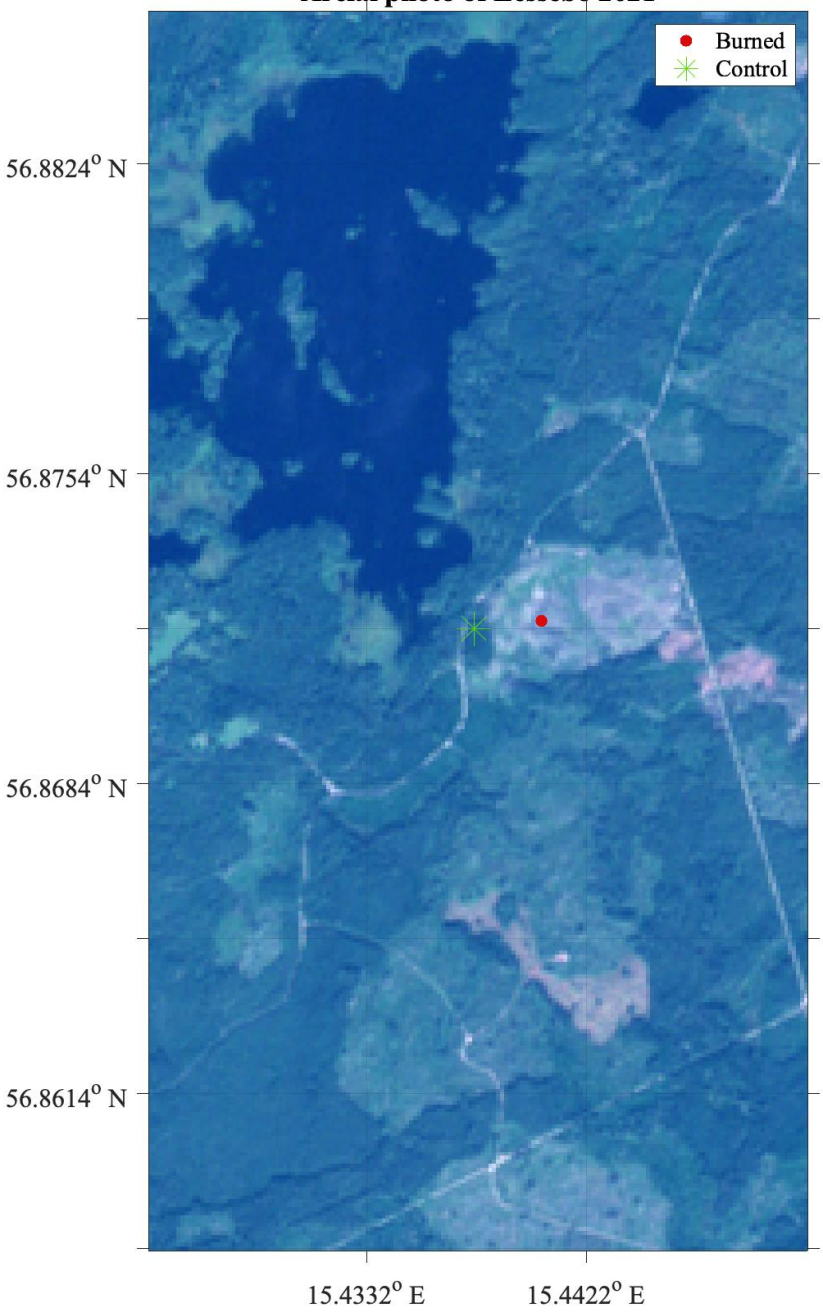

Appendix VIII: Photographs from the sites

Photographs of all sites used in the study at the time of coring. The photographs show the forest subcanopy for control and burned plot. The site Rullerum does not have control photos, thus, only the burn plot is visible. All photos were taken by Joanna Eaton (© Joanna Eaton 2022).

VIII.I. Kil Control

VIII.II. Kil Burnt

VIII.III. Rullerum Burnt

VIII.IV. Österbymo Control

VIII.V. Österbymo Burnt

VIII.VI. Stormandebo Control

VIII.VII. Stormandebo Burnt

VIII.VIII. Lessebo Control

VIII.IX. Lessebo Burnt